

Alma Mater Studiorum – Università di Bologna

DOTTORATO DI RICERCA IN  
Scienze Biomediche e Neuromotorie

Ciclo XXXII

**Settore Concorsuale:** 05/D1

**Settore Scientifico Disciplinare:** BIO/09

TOWARD A FULL PREHENSION DECODING FROM  
DORSOMEDIAL AREA V6A

**Presentata da:** MATTEO FILIPPINI

**Coordinatore Dottorato**

PROF. PIETRO CORTELLI

\_\_\_\_\_  \_\_\_\_\_

**Supervisore**

PROF.SSA PATRIZIA FATTORI

\_\_\_\_\_  \_\_\_\_\_

**Esame finale anno 2019**

# Index

Index .....	1
1. Abstract .....	3
2. Introduction .....	5
2.1. Posterior Parietal Cortex (PPC) .....	8
2.2. Area V6A of macaque PPC .....	10
2.3. Cognitive Neural Prosthetics from PPC .....	13
2.4. Aim of the thesis: decoding full prehension signals from V6A for cognitive BCIs .....	15
3. Decoding information for grasping from the macaque dorsomedial visual stream .....	18
3.1. Abstract .....	18
3.2. Introduction .....	19
3.3. Materials and Methods .....	20
3.3.1. Experimental procedure .....	20
3.3.2. Behavioral task .....	21
3.3.4. Tested objects .....	22
3.3.5. Data analysis .....	23
3.3.6. Population response .....	24
3.3.7. Neural Decoding .....	24
3.4. Results .....	28
3.4.1. Decoding results .....	31
3.4.2. Object recognition within the object presentation epoch .....	32
3.4.3. Time-course of the decoding performance .....	34
3.4.4. Generalization analysis .....	36
3.5. Discussion .....	39
3.5.1. Offline decoding from single cells in dorso-medial fronto-parietal areas: perspectives on BCIs ..	41
3.5.2. Future directions .....	42
4. Prediction of reach goals in depth and direction from the parietal cortex .....	43
4.1. Summary .....	43
4.2. Introduction .....	44
4.3. Results .....	46
4.3.1. Whole epoch decoding .....	46
4.3.2. Neuron Dropping Analysis .....	47
4.3.3. Time course of the decoding performance .....	48
4.3.4. Generalization analysis .....	50
4.4. Discussion .....	51

4.4.1. Decoding reach goals from parietal cortex .....	52
4.4.2. Decoding of depth information for reaching.....	53
4.4.3. Decoding entire prehension from V6A.....	54
4.4.4. Potential applications and future directions .....	54
4.5. Experimental procedures .....	55
4.5.1. Experimental procedure .....	55
4.5.2. Equipment and Behavioral Task .....	55
4.5.4. Neural decoding .....	56
4.6. Supplemental Experimental Procedures.....	57
4.6.1. Behavioral task .....	57
4.6.2. Control task .....	58
4.6.3. Neuron dropping. ....	59
4.6.4. Sliding window decoding.....	59
4.6.5. Generalization analysis.....	60
4.6.6. Population response.....	60
4.6.7. Comparison between the results of Fixation-to-reach task and Constant-gaze task. ....	60
4.7. Supplemental Figures .....	61
Figure S1 .....	61
Figure S2 .....	62
5. General discussion.....	64
5.1. PPC for decoding .....	65
5.2. Full prehension .....	67
5.3. Limitations and Future directions .....	68
6. Conclusions.....	70
7. Bibliography.....	71

## 1. Abstract

Neural prosthetics represent a promising approach to restore movements in patients affected by spinal cord lesions. Intact signals recorded from cerebral cortex can be decoded and used to drive neural prostheses. Understanding how the brain codes information and how different cortical areas could contribute to prosthesis operation is still a critical point. To drive a full capable, brain controlled, prosthetic arm, reaching and grasping components of prehension have to be accurately reconstructed from neural activity. The posterior parietal cortex (PPC) mediates sensorimotor transformations, spatial attention, and motor planning. In PPC several areas encode for different aspects of prehension acts, with reaching and grasping often assigned to separate regions. PPC signals were already used in a clinical trial on paraplegic patients to move a prosthetic arm. Two implants have been placed on different areas to use on one side reach directional signals and on the other grip related information, and still the prosthetic movement was slow and clumsy.

Neurons in the dorsomedial area V6A of macaque show sensitivity to reaching direction accounting also for depth dimension, thus encoding positions in the entire 3D space. Moreover, many neurons are sensible to grips types and wrist orientations. To assess whether these signals are adequate to drive a full capable neural prosthetic arm, we recorded spiking activity of neurons in area V6A, spike counts were used to train machine learning algorithms to reconstruct reaching and grasping. In a first work, two *Macaca fascicularis* monkeys were trained to perform an instructed-delay reach-to-grasp task in the dark and in the light toward objects of different shapes. Population neural activity was extracted at various time intervals on vision of the objects, the delay before movement, and grasp execution. The activity of 89 neurons was used to train and validate a Bayes classifier used for decoding objects and grip types. Recognition rates were well above chance level for all the epochs analyzed in this study. In a second work, monkeys were trained to perform reaches to targets located at various depths and directions and the classifier was tested whether it could correctly predict the reach goal position from V6A signals. The reach goal location was reliably decoded with accuracy close to optimal (>90%) throughout the task. I then compared population-level representation along task using a generalization approach; that is, I trained a decoder on the spike data from the initial fixation and then tested its performance on the data from the movement interval. This was useful to study the dynamics of sensorimotor transformations. For both reaching and grasping, codes progressively evolve from a visual (spatial) to motor encoding with a mixed code during the delay period before movement execution.

Together these results, show a reliable decoding of hand grips and spatial location of reaching goals in the same area, suggesting that V6A is a suitable site to decode the entire prehension action with obvious advantages in terms of implant invasiveness. This new PPC site useful for decoding both reaching and grasping opens new perspectives in the development of human brain-computer interfaces.

## 2. Introduction

During our entire life, we constantly interact with surrounding objects. Reaching for food, handling tools at work, playing with our children or helping our relatives. All these natural activities require complex interactions driven by our nervous system that finely controls body effectors. However, unpredictable events could dramatically hinder everyday activities. A car crash can be the cause of severe spinal cord injury (SCI) that can often result in the permanent loss of functions, causing enormous personal, social and economic problems. A recent report from American National Spinal Cord Injury Statistical Center (National Spinal Cord Injury Statistical Center, Birmingham, 2018) stated an annual incidence of spinal cord injury (SCI) approximately of 54 cases per one million people in the United States, with 17,730 new SCI cases each year. In Europe, an estimated number of 330,000 people are living with the consequences of spinal cord injury, with 11,000 new injuries occurring per year (Rupp, 2014). The bilateral loss of the grasp function in individuals suffering from a cervical SCI severely limits the affected individuals' ability to live independently and retain gainful employment post injury. Therefore, one of the main priorities of these patients is to improve a missing grasping and reaching function (Anderson, 2004; Simpson et al., 2012; Collinger et al., 2013).

Although nerve regeneration may be a possible solution, a deep understanding of molecular basis of tissue regeneration is still missing and clinical applications are still far (Young, 2014; Sofroniew, 2018). Brain Computer Interfaces (BCIs) offer a viable alternative, with promising human applications (Hochberg et al., 2012; Collinger et al., 2013; Aflalo et al., 2015). BCIs record bioelectrical signals generated by brain circuits, these signals are informative about volitional movement. Next, a computer algorithm, the neural decoder, translates recorded brain activity into signals capable of driving prosthetics (effector). Neural prosthetic is 'mind controlled' and under strict control of patient to replace the real body and restore mobility (Fig. 1). Critical points of BMI technology are the bandwidth between the brain and the decoder (this is related to the number of recording channels), and the ability of the decoder to extract key information to move correctly each of prosthetic's degrees of freedom (DOF). Different input have been used to drive BMIs: EEG, ECoG and fMRI signals (Rupp, 2014; Bockbrader et al., 2018) but intracortical recording outperform others in term of temporal resolution and signal to noise ratio (Waldert, 2016). Temporal resolution is a key point to return a natural feeling to BMI user. Downside of intracortical recordings is implant invasiveness (Murphy et al., 2016).

The current state of art for human cortical recording is the Utah Array, a 96 multielectrode array, 4x4mm size (Fig. 1.1), inserted in the cortex and connected to a dock fixed on the patient skull. Connector pins are exposed to enable a direct link between electrodes and amplifier. Moreover, insertion of electrodes within the cortex triggers inflammatory response, which ultimately reduces signals yield over time (Kozai et al., 2015; Salatino et al., 2017). Increasing the number of electrodes to sample more and more neurons is still possible, yet a fair trade-off between number of neurons required to dexterously drive a BMI and implant invasiveness should be pursued.

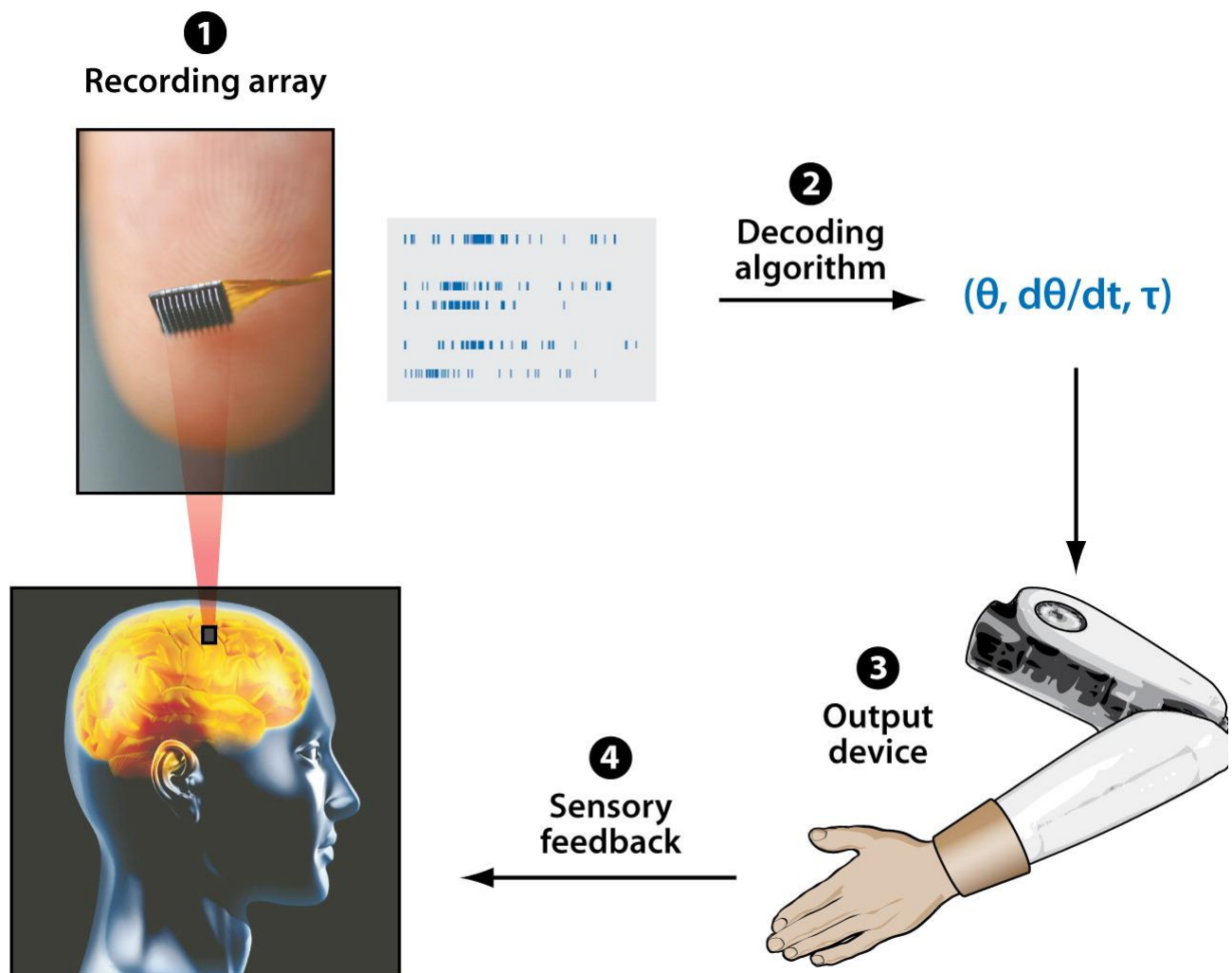


Figure 1. Main components of a neural interface system: (1) a recording array that extracts neural signals, (2) a decoding algorithm that translates these neural signals into a set of command signals, (3) an output device that is controlled by these command signals, and (4) sensory feedback in the form of vision and potentially other sensory modalities. Figure modified from (Hatsopoulos and Donoghue, 2009).

Extracting high valuable information from brain regions strictly correlated with the movement, helps to reduce the number of recording channels needed to efficiently drive neural prosthetic. Signals from different human brain regions were successfully used to decode motor intentions and actions in neuroprosthetic. The first attempts demonstrated that it was possible drive a full 7 DOF robotic arm using signals from motor cortex (Collinger et al., 2013) (Fig. 2ABC). Motor cortex signals give easy access to information on arm position, velocity and acceleration (Georgopoulos et al., 1982; Schwartz, 1994; Paninski et al., 2004). Given the rich repertory of movement our limbs can perform (our hand is capable of 22 DOF), many channels are required to extract this information in detail. In contrast to motor BCIs, BCIs based on signals from upstream areas like PPC have intriguing attractions (cognitive BCI). Aflalo and colleagues showed that also signals from posterior parietal cortex (PPC) were adequate to drive a high DOF prosthesis (Aflalo et al., 2015) (Fig. 2DE). Indeed, PPC is implicated in the processing of spatial awareness, attention and action planning (Galletti and Fattori, 2018; Gallivan and Goodale, 2018), information is here encoded in a more abstract form but still available, not linked to a specific effector and is described with few neurons (Andersen et al., 2010, 2014).

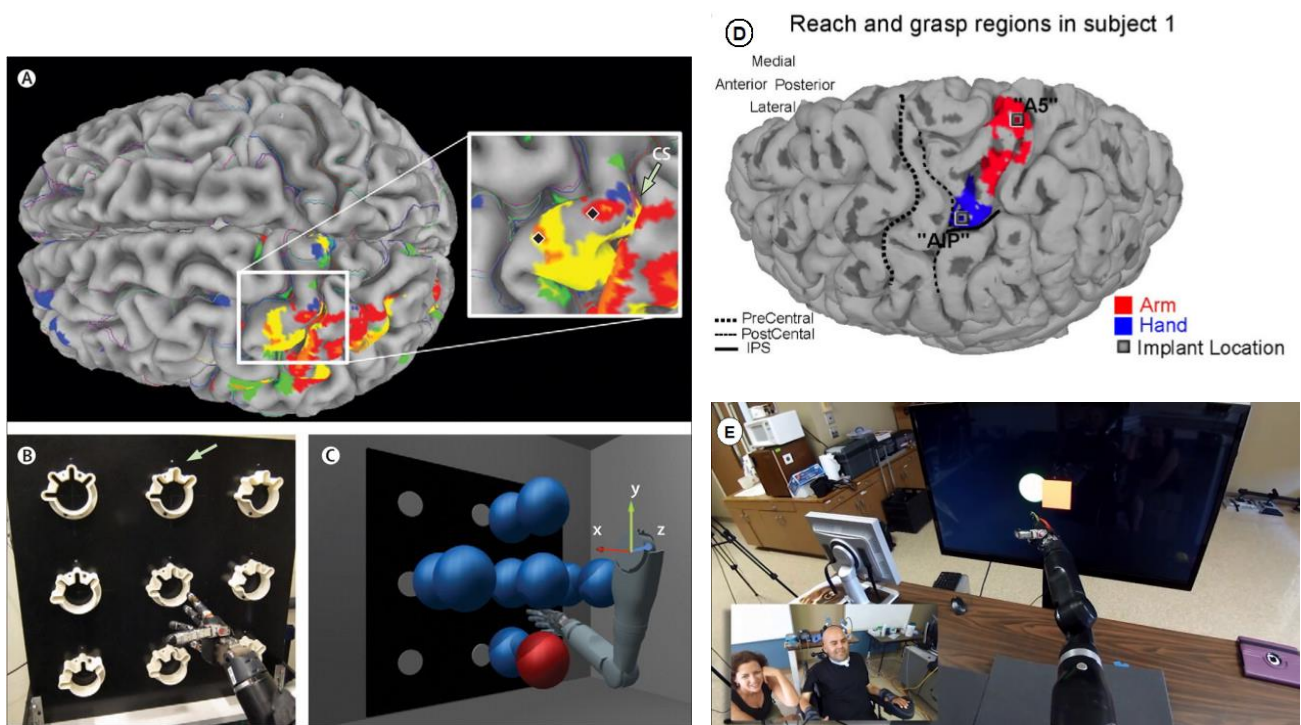


Figure 2. (A) Array location and preoperative functional MRI activation maps of a participant specific brain model during video-guided attempted movement. The colors in the activation maps represent blood-

oxygenation-dependent activities during video-guided attempted movements. Two Utah arrays were implanted in primary motor cortex. (B) Neural control of a prosthetic limb with signals from human motor cortex. (C) Diagram of the prosthetic limb and translation targets (red and blue spheres) for the seven-dimensional sequence task. (D) Functional results rendered on a reconstructed cortical surface. Areas with significantly greater activation for the reach condition (red) as compared to areas showing greater activation for the grasping condition (blue). In opposition to (A) where arrays were placed into motor cortex, here PPC was targeted: a first array was implanted in area BA5, the second array in human anterior intraparietal area (AIP). (E) Neural control of a prosthetic limb with signals from human posterior parietal cortex. CS=central sulcus. Figures A, B, C modified from Collinger et al. 2013, figures D, E, from Aflalo et al. 2015.

## 2.1. Posterior Parietal Cortex (PPC)

The posterior parietal cortex provides a bridge between sensory areas in the caudal cortex and motor areas in more rostral cortex. Neurons in this region cannot be classified as simply sensory or motor, but rather they have properties of both and are involved in sensorimotor transformation. According to the “Two Visual Systems Hypothesis” (Goodale and Milner, 1992) visual information flows from the primary visual cortex to several areas of the extrastriate visual cortex along two separate channels called the dorsal and ventral visual streams (Ungerleider and Mishkin, 1982). The dorsal visual stream leads toward the PPC where visual information is mainly exploited to guide action. Alternatively, the ventral visual stream projects toward the inferior temporal cortex, where visual information is analyzed for the purpose of recognizing, analyzing, and categorizing visual objects (Milner and Goodale, 2006). Within the dorsal visual stream, different areas have attracted attention of the scientific community. For example, AIP has been associated with the control of hand-object interactions required for grasping, LIP for the guidance of eye movements (Taira et al., 1990; Gallese et al., 1994; Murata et al., 2000; Cui and Andersen, 2007; Gardner et al., 2007; Sakata et al., 2012). In opposition, planning and execution of reaching movements involve mainly areas of the superior parietal lobe (Snyder et al., 1997; Battaglia-Mayer et al., 2000, 2007; Fattori et al., 2005; McGuire and Sabes, 2011; Hadjimitsrakakis et al., 2012, 2015).

The traditional model, considered valid till recently (Fig. 3, Kandel et al., 2013), separates reaching and grasping processing in two different parietal-frontal networks within the dorsal visual stream: the dorso-medial belongs to the reaching network, the dorso-lateral to the grasping network (Jeannerod and Decety, 1995; Matelli and Luppino, 2001). Accordingly, reach-related signals flow from the superior parietal areas to the dorsal premotor cortex, grasp-related signals are conveyed from lateral parietal cortex to ventral premotor cortex. Finally, both streams converge on the

primary motor cortex (Burman et al., 2014; Dea et al., 2016). However, recent literature reported that grasping parameters can be coded in the traditionally reaching domains of the superior parietal cortex (Chen et al., 2009; Fattori et al., 2010), or single neurons from anterior intraparietal area (AIP) encoded both the reaching direction and grip type (Lehmann and Scherberger, 2013). Also premotor areas show bimodal encoding of reaching and grasping information (Raos et al., 2004; Stark et al., 2007). In the light of these new results traditional models should be updated.

The superior parietal lobule (SPL) is located in the medial part of PPC. SPL hosts several areas: PE and PEc, located nearby on the exposed surface of SPL, area PGm (or 7 m), on the mesial surface of the hemisphere, MIP in the medial bank of intraparietal sulcus, area V6A, located posterior to PEc and hidden in the parieto-occipital sulcus. All these areas have been implicated in arm reaching movements (Ferraina et al., 1997; Snyder et al., 1997; Battaglia-Mayer et al., 2001; Fattori et al., 2001, 2005; McGuire and Sabes, 2011; Hadjidimitrakis et al., 2015; De Vitis et al., 2019). Area V6A, in the caudal part of SPL, is a crucial node of the dorsal visual stream, at the origin of several pathways for visuo-spatial processing and hand action control (Rizzolatti and Matelli, 2003; Kravitz et al., 2011; Galletti and Fattori, 2018).

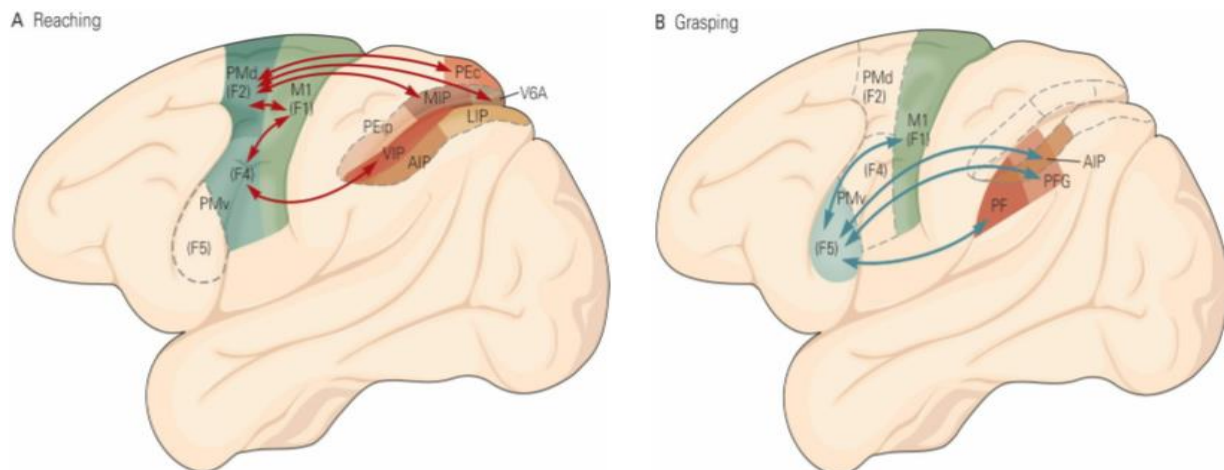


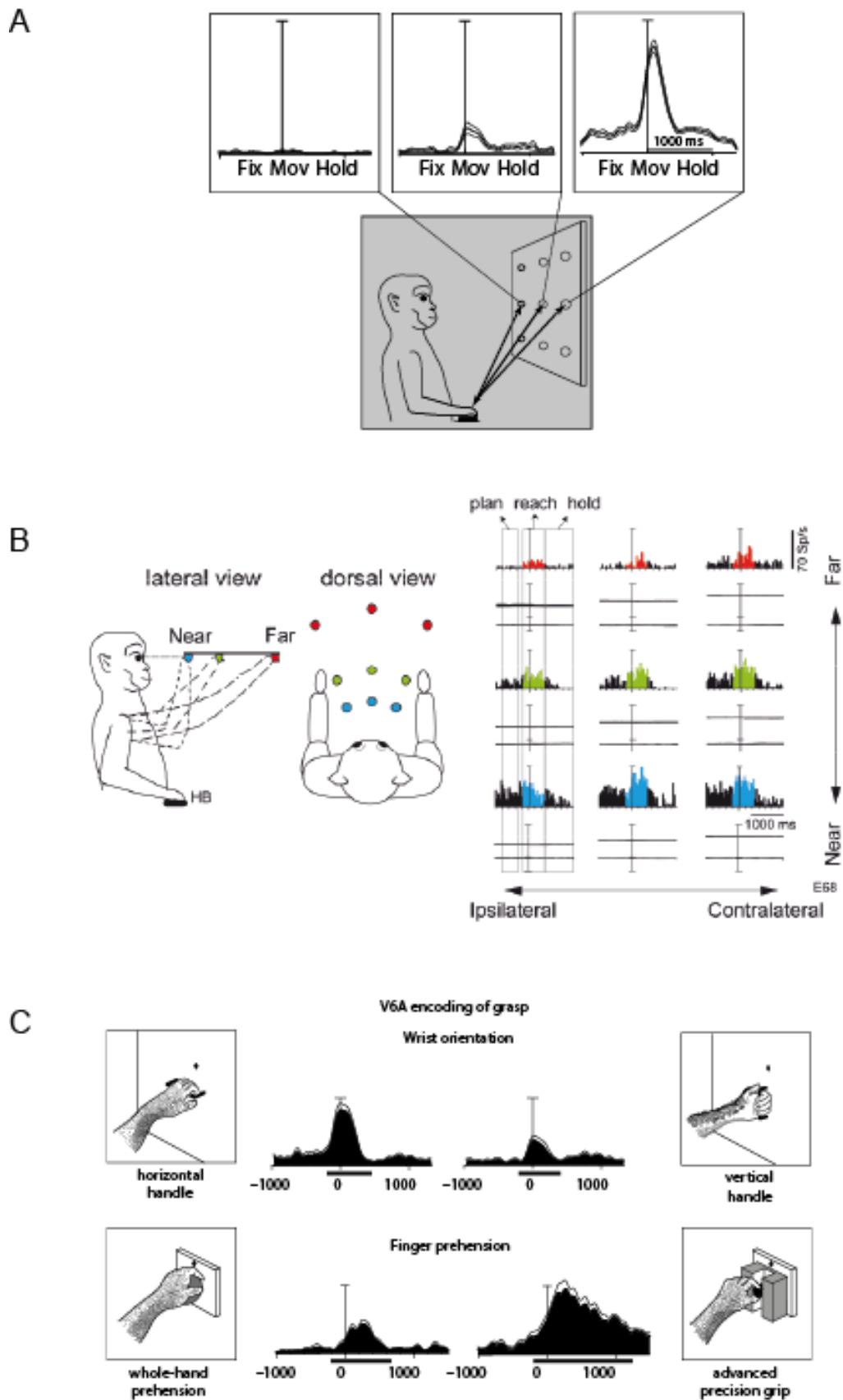
Figure 3. The traditional view separates parieto-frontal pathways involved in the visuomotor transformations for reaching and grasping. A. The visuomotor transformation necessary for reaching is mediated by the parietofrontal network shown here. The areas located within the intraparietal sulcus are shown in an unfolded view of the sulcus. Two serial pathways are involved in the organization of reaching movements. The ventral stream has its principal nodes in the ventral intraparietal area (VIP) and area F4 of the ventral premotor cortex, whereas the dorsal stream has synaptic relays in the superior parietal lobe (MIP, V6A) and the dorsal premotor cortex (PMd), which includes area F2. (Parietal areas include AIP, anterior intraparietal area; LIP, lateral intraparietal area; and V6A, the parietal portion of the parieto-occipital area.) B. The visuomotor transformations necessary for grasping is mediated by the parieto-frontal

network shown here. The AIP and PFG areas are concerned mostly with hand movements, whereas area PF is concerned with mouth movements. Area F5 in PMv is concerned with both hand and mouth motor acts. Some grasping neurons have been found in F2, the ventral part of PMd. Area M1 (or F1) contains a large sector that controls the fingers, hand, and wrist. Figure modified from Kandel 2013.

## 2.2. Area V6A of macaque PPC

V6A is a visuomotor area that contains about 60% of visual neurons, about 30% of somatic cells, about 70% of V6A cells show arm movement-related activity and approximately 60% of neurons are sensitive to wrist orientation and to grip formation (Gamberini et al., 2011). The receptive fields of visual cells cover a large part of the visual field, but retinotopic organization is not clear and nearby neurons often represent different parts of the visual field (Galletti et al., 1999a). The representation of the lower contralateral quadrant is particularly emphasized, the strong representation of lower part of visual field is indicative for an advantageous reaching planning and control. Somatic receptive fields are denser for the proximal part of the arm, a smaller fraction on the distal segment, including the hand, with the head and legs not represented. Proprioception (75% of neurons) is more strongly represented than touch (25%) (Breveglieri et al., 2002). The richer representation of the arm joints in V6A points toward a strong involvement of arm reaching movements which requires somatosensory information for a finer control. What is more relevant for neuro prosthetic control are the motor-related properties of area V6A. Indeed, most of the neurons of V6A are tuned by reaching and grasping movements (Gamberini et al., 2011). In reaching neurons, the neural discharge is tuned by the direction of arm movement (Fattori et al., 2005, Fig. 4A) and by the distance reached by the hand (Hadjidimitrakis et al., 2014a, 2015). In figure 4B an example of a reaching-related V6A neuron showing an activity modulation according to different depth levels. In V6A presence or absence of visual feedback can modulate neuronal activity, comparing reaching of targets performed in dark versus light conditions different neural subpopulations can be identified. Neurons insensitive to visual background have been labeled motor neurons, yet visuomotor neurons show peculiar modulations depending on availability of visual information (Bosco et al., 2010). The presence of these separate classes of cells suggests that V6A may be involved in a system able of comparison of the motor plan with current sensory feedback produced by the moving arm, this system could handle online control of movements.

V6A also contains neurons sensitive to wrist orientation (Fattori et al., 2010) and the grip used by the animal to grasp the object (Fattori et al., 2010, 2012). In figure 4C there is an example of neuron coding for wrist orientation (top) and another neuron modulated by grip type (down). In contradiction with the model of two separate networks for reach and grasping (Jeannerod, 1986; Kandel et al., 2013), V6A hosts neurons coding both transport and grip components of prehension. Moreover, when the same neurons were tested for both reaching directions and wrist orientation, 75% of neurons sensitive to reach were also modulated by different wrist orientations (Fattori et al., 2009). Thus, area V6A is involved in all aspects of reach to grasp movements supporting the whole prehension (Fattori et al., 2017).



rectangle) toward one of three targets located on a panel in front of the animal. The task was a foveal reach toward a visual target. Three time intervals were of particular interest: *Fix*, the monkey was fixating the target and no interactions were required, *Mov*, the monkey performed the reach toward the target, *Hold*, the hand was held on target button. An increase in discharge for the right position indicates a clear spatial tuning for right reach direction. Modified from Fattori et al. 2005. (B) Spatial signals for reaching in V6A. Left: experimental set-up used for testing reaching discharges when the arm is directed towards different directions and depths (different colors: near is blue, far is red). Eye and hand movements are performed toward one of the 9 targets located at eye level at different depths and directions. Right: Example neuron with depth tuning in several epochs. From top to bottom in each panel: spike histograms, version (1st trace) and vergence (2nd) eye traces. The 9 panels illustrate neural responses and eye signals for the 9 target positions arranged in 3 directions (columns) and 3 depths (rows). Vertical bars indicate the alignment of neural activity and eye traces at the start of arm movement. In color: the epochs coincident with the execution of reaching: red is the farthest, blue the nearest. Spatial modulations occur during both planning and execution of arm movement, showing a preference for reaches towards targets near the body. Modified from Fig. 3 of Hadjimitsakis et al., 2014. (C) V6A grasp-related properties. Two examples of cells modulated by wrist orientation (top) and by finger prehension (bottom). Horizontal bars below the spike density functions indicate the duration of the movement epoch considered. On the sides, the sketches of the hand actions performed by the monkey are shown. Modified from Fattori et al. (2009, 2010).

### 2.3. Cognitive Neural Prosthetics from PPC

Cognitive neural prosthetic relates not to the brain location of the recording but rather the type of signal that is being extracted (Andersen et al., 2004, 2010). Motor imagery, planning, attention, decision making are examples of signals that could support cognitive neural prosthetic. In associative cortical areas this information is broadly represented. As PPC is implicated in sensory-motor integration, this region is particularly interesting for the extraction of cognitive signals supporting movement planning and control. So far, most of neural prosthetic applications focused on decoding trajectory to move a cursor or a robotic arm to a goal (Taylor et al., 2002; Carmena et al., 2003; Serruya et al., 2003). However full neural control of prosthetic arm is still far to be optimal, movements are slow and clumsy (Collinger et al., 2013; Wodlinger et al., 2015; Downey et al., 2017). An alternative approach is extracting information from areas that carry the intention to make movements at a higher cognitive level like PPC, movement trajectories could be reconstructed with computer vision algorithms.

PPC signals are particularly advantageous for neuro prosthetic control. Neurons in this region often encode for movement goals, but also Baldauf and colleague found that two goals and their sequence were represented simultaneously (Baldauf et al., 2008). This could be convenient to instruct the prosthetic arm to quickly perform complex movements. Furthermore, PPC can also encode trajectories, combining decoding of trajectory with decoding of reaching goal helps to

build a more robust model (Mulliken et al., 2008a). Another advantage in using PPC signals is the bilateral representation of limb movement (Quiñero et al., 2006; Chang and Snyder, 2012); although to a certain extent this is also present in primary motor cortex (Donchin et al., 1998), in PPC representation of limbs is continuous from pure contralateral to bimanual (Chang et al., 2008). Alternative to spikes, local field potentials (LFPs) are acquired from raw voltage signals. LFPs average electrical fields generated from thousands of neurons firing simultaneously (Buzsáki et al., 2012). Specific frequency bands are correlated with motor control and could be used as input for neural decoding (Spinks et al., 2008; Zhuang et al., 2010; Bansal et al., 2012; Flint et al., 2012; Stavisky et al., 2015). Local field potentials are very strong in PPC and could be used to improve decoding performance combined with single unit activity, or when deterioration of single unit yield arises (Hwang and Andersen, 2013). This is another reason to choose PPC for cognitive BCIs.

Different PPC areas were successfully used to decode motor intentions mostly in monkey, but also in humans. The parietal reach region (PRR), roughly located in caudal SPL, was defined on functional basis as a region encoding the direction of reaching movement, as well as the intention to move the arm (Snyder 1997). Area 5d is located on the gyral surface in monkey and humans, encodes for reaching goals and trajectories. Neurons from monkey area 5d were used to volitionally move a cursor on a computer screen (Mulliken et al., 2008a) and a 3D space (Hauschild et al., 2012). A tetraplegic patient implanted with a 96 electrodes in putative human area 5d was able to control the position of a robotic arm (Fig. 2DE, Aflalo et al., 2015). The same patient was implanted with a second array in human putative area AIP. Previous study on monkeys found neurons in area AIP sensitive to objects shape and hand configurations required to grasp them (Murata et al., 2000; Schaffelhofer et al., 2015). Also from human AIP it was possible the decoding of 5 stereotyped hand configurations (Klaes et al., 2015). Located on the lateral wall of caudal intraparietal sulcus, area LIP in monkey encodes for saccades. The target of a reaching movement often coincided with gaze position, thus saccade decoding could support decoding of reaching (Graf and Andersen, 2014). Saccade-related and gaze position signals have been demonstrated to be important not only for reaching movement, but also for orienting responses i.e. coordinated eye-head movements (Hadjidimitrakakis et al., 2019).

## 2.4. Aim of the thesis: decoding full prehension signals from V6A for cognitive BCIs

As summarized above, neurons in dorsomedial area V6A of monkey encode for different aspects of reach-to-grasp actions. Neural discharge in this area is tuned by the direction of arm movement (Fattori et al., 2005) and by the distance reached by the hand (Hadjidimitrakis et al., 2011, 2014b). V6A also contains neurons sensitive to wrist orientation (Fattori et al., 2009) and the grip used by the animal to grasp the object (Fattori et al., 2010, 2012). A single area that encodes for all aspects of reach-to-grasp actions is of great interest for BCI applications, indeed a single electrodes array inserted in area V6A could potentially extract all the information needed to drive a prosthetic arm under volitional control of the patient. To reach this goal, the first step is to decode signals for the entire prehension from V6A. In this thesis an extensively decoding analysis is proposed with the final goal of understanding whether V6A signals are virtually capable to drive a neuro prosthetic arm. To convert information encoded by neurons as firing rates into more computer friendly variables (decoding process), peculiar computer algorithms are trained to recognize firing rate patterns and to relate them with the investigated motor aspect (e.g. reaching direction or grasp type). Neural decoding is a critical step in BCI technology: this process aims to convert high-dimensional neural data (number of neurons recorded) to a lower dimension representation. The output signals could be used to drive prosthetic limbs, in this case, the number of reduced dimensions which represent neural activity usually match with the degrees of freedom of prosthesis. Neural decoding is a valuable tool not only for neural prosthetic applications, but also to study the neural representation of cognitive functions, expressing the ongoing neural activity of recorded population in a reduced and more readable form.

To the purpose of using signals from V6A, we first recorded spiking activity of single neurons of area V6A of monkey. Then neural datasets were used to train a neural decoder to retrieve spatial position of 3D reaching goals, a second dataset was used to decode the types of grips. Having decoded both reach and grasp component of prehension we studied whether signals from area V6A may possibly support neural prosthetic applications.

To obtain spiking activity of single neurons intracortical recording are required. In intracortical recording, acquisition system records electric potential difference from electrodes inserted within the cortex. Signals from electrodes are amplified and action potential of single neurons are detected with a spike sorting process. Most of neural decoders assume that information is contained in neuron spiking rate. Accordingly timing of action potentials are binned in small time

intervals. An alternative way is to model precise spike time as important, temporal coding is a significant element in neural coding (Thorpe, 1990; Gautrais and Thorpe, 1998) but rate coding seems to be a fair approximation of ongoing neural activity (Stein et al., 2005). Rate coding was assumed in my analysis.

Several decoding algorithms have been used to decode motor and cognitive aspects of reach-to-grasp movements. From the simplest to the most complex, it does not exist a best decoding algorithm, instead each algorithm has its strengths to adapt to the context where applied to solve a particular problem. For example, neurons from primary motor cortex could be described using a cosine tuning function while the monkey move a manipulandum to one of eight different directions (Georgopoulos et al., 1982). Each neuron has a preferred direction (phase offset), the firing rate of each neuron is used to describe its preferred direction vector, the sum of all vectors over the population (population vector) is the lower dimensional output. Although this is the simplest decoding algorithm that could be described, it was shown to be successful in monkeys (Serruya et al., 2002; Taylor et al., 2002; Carmena et al., 2003; Jarosiewicz et al., 2008; Velliste et al., 2008) and also allowed a tetraplegic human patient to move a prosthetic arm (Collinger et al., 2013; Wodlinger et al., 2015). Kalman filter can take advantage of cosine tuning of neurons, this recursive algorithm has been implemented for controlling a cursor on a computer monitor (Jarosiewicz et al., 2008; Kim et al., 2008; Simeral et al., 2011; Gilja et al., 2015) and volitional control of a robotic arm (Hochberg et al., 2012). Firing rate can be also modeled as a time-evolving hidden variable using a hidden Markov model. Hidden variables are cognitive states or target goals to be decoded (Kemere et al., 2008).

In the proposed analysis, a different class of neural decoder were used. Thanks to the increase in computational power of the last decades, machine learning algorithms are a valid alternative to linear methods previously described. These algorithms are intelligent in the way that they can learn patterns in big dataset and find non-linear correlation between input and dimension reduced output. Neural datasets, given their intrinsic high dimensionality (each recorded neuron is a dimension), are well suited to being analyzed with machine learning techniques. Here we used naïve Bayes classifiers to reconstruct from population firing rates: 1) the spatial position of reaching goals or 2) the correct grip type used by the monkey during a grasping task. I found that both reaching and grasping can be decoded with very high accuracy throughout the task execution. These results support a decoding of full prehension from area V6A. Here I suggest that

decoded signals from V6A can be exploited to control reaching and grasping aspects of a prosthetic limb. In the following chapters, two works I first authored are reported, with all the details of these studies.

### 3. Decoding information for grasping from the macaque dorsomedial visual stream

MATTEO FILIPPINI<sup>1\*</sup>, ROSSELLA BREVEGLIERI<sup>1\*</sup>, M. ALI AKHRAS<sup>1</sup>, ANNALISA BOSCO<sup>1</sup>, ERIS CHINELLATO<sup>2</sup>, PATRIZIA FATTORI<sup>1</sup>;

<sup>1</sup>Dept. Pharmacy and Biotechnology, Univ. of Bologna, 40126 Bologna, Italy; <sup>2</sup>School of Science and Engineering, Middlesex University, London NW4 4BT, United Kingdom

\* These authors equally contributed to this work

#### 3.1. Abstract

Neuro-decoders have been developed by researchers mostly to control neuro-prosthetic devices, but also to shed new light on neural functions. In this study, we show that signals representing grip configurations can be reliably decoded from neural data acquired from area V6A of the monkey medial posterior parietal cortex (PPC). Two *Macaca fascicularis* were trained to perform an instructed-delay reach-to-grasp task in the dark and in the light towards objects of different shapes. Population neural activity was extracted at various time intervals; on vision of the objects, the delay before movement, and grasp execution. This activity was used to train and validate a Bayes classifier used for decoding objects and grip types. Recognition rates were well over chance level for all the epochs analyzed in this study. Furthermore, we detected slightly different decoding accuracies depending on the task's visual condition. Generalization analysis was performed by training and testing the system during different time intervals. This analysis demonstrated that a change of code occurred during the course of the task. Noteworthy, the ability of our classifier to discriminate grasp types was fairly well in advance with respect to grasping onset. This feature might be important when the timing is critical to send signals to external devices before the movement start. Our results suggest that the neural signals from the dorsomedial visual pathway can be a good substrate to feed neural prostheses for prehensile actions.

## 3.2. Introduction

Artificial systems have not yet achieved the ability of the primate hand to reach, grasp and manipulate objects. The fine performance of the human hand has also inspired research on humanoid robots in order to achieve dexterous grasping and manipulation of objects (Mattar, 2013; Chinellato and del Pobil, 2016). Decoding neural population signals from motor-related areas of the monkey, and recently from human brains, constitutes a promising way to implement modern Brain-Computer Interfaces (BCIs) able to finely control arm actions (Wessberg et al., 2000; Serruya et al., 2002; Taylor et al., 2002; Carmena et al., 2003; Musallam et al., 2004; Santhanam et al., 2006; Schwartz et al., 2006; Hochberg et al., 2006, 2012; Kim et al., 2006; Fetz, 2007; Mulliken et al., 2008a; Velliste et al., 2008; Nicolelis and Lebedev, 2009; Scherberger, 2009; Hatsopoulos and Donoghue, 2009; Carpaneto et al., 2011; Shenoy et al., 2011; Townsend et al., 2011; Collinger et al., 2013; Sandberg et al., 2014; Aflalo et al., 2015; Schaffelhofer et al., 2015; Milekovic et al., 2015; Schwartz, 2016).

The medial subdivision of the dorsal visual stream (dorsomedial fronto-parietal network, Galletti *et al.*, 2003) has traditionally been considered as being involved in controlling the transport component of prehension (Caminiti et al., 1996; Jeannerod, 1997; Wise et al., 1997) and its neuronal activity has been successfully exploited to decode reach endpoints, goals and trajectories (Hatsopoulos et al., 2004; Musallam et al., 2004; Santhanam et al., 2006; Mulliken et al., 2008a; Aggarwal et al., 2009; Chinellato et al., 2011; Aflalo et al., 2015). However, the dorsomedial stream has also been determined recently as one of the candidate cortical areas involved in encoding grasping (Raos et al., 2004; Stark et al., 2007; Fattori et al., 2010; Breveglieri et al., 2016). This opens new perspectives on the problem of neural signal decoding for hand configurations. In the present work, we analyzed the decoding potential of a parietal node of the dorsomedial stream (area V6A, Galletti *et al.*, 1999) for grasping actions.

Neural decoding analyses typically have two complementary objectives: selecting potential brain areas for driving BCIs, and achieving a deeper understanding of the function of neurons in the studied region. In particular, we wanted to ascertain whether the same neural code is employed throughout a grasping task, or if it changes within the time-course of the action generation. We applied a generalization analysis to investigate this issue. The system was trained and tested during different time intervals, and, to the best of our knowledge, has never been employed before in related studies.

In addition, we wanted to investigate the dependence of the decoding performance of the proposed neuro-decoder on the task condition; more precisely, when grasping is planned and executed either in the dark or in the light. Recent papers show that in V6A there is an interplay between vision and movement, both in reaching (Bosco et al., 2010) and in grasping (Breveglieri et al., 2016), given that most V6A cells are modulated by both motor-related and visual components. We wanted to see whether there are differences in decoding performance when the visual information is present or absent before and during grasping and, in that case, to look for differences in the time course of the neural codes employed by V6A cells during the preparation and execution of grasping actions in the dark and in the light.

The results of our analysis show that V6A neural signals can be reliably used to decode grasps, and that the neural code used by V6A cells during object vision is not maintained during the subsequent phases of the task (i.e., grasping preparation and execution), where a different code is employed. We demonstrated that the neuro-decoder performance is slightly influenced by the presence of visual information regarding the object to be subsequently grasped and regarding the hand-object interaction, which gives a clear view of the role of vision before and during grasping in V6A.

### 3.3. Materials and Methods

#### 3.3.1. Experimental procedure

The study was performed in accordance with the guidelines of the EU Directives (EU 116-92; EU 63-2010) and the Italian national law (D.L. 116-92, D.L. 26-2014) on the use of animals in scientific research. During training and recording sessions, particular attention was paid to any behavioral and clinical sign of pain or distress. We involved two male *Macaca fascicularis* monkeys, weighing 3.650 and 2.450 kg. A head-restraint system and a recording chamber were surgically implanted in asepsis and under general anesthesia (sodium thiopental, 8 mg/kg/h, *i.v.*) following the procedures reported in (Galletti et al., 1995). Adequate measures were taken to minimize pain or discomfort. A full program of postoperative analgesia (ketorolac trometazyn, 1mg/kg *i.m.* immediately after surgery, and 1.6 mg/kg *i.m.* on the following days) and antibiotic care

(Ritardomicina<sup>®</sup> (benzatinic benzylpenicillin plus dihydrostreptomycin plus streptomycin) 1-1.5 ml/10kg every 5-6 days) followed the surgery.

We performed extracellular recordings from the posterior parietal area V6A (Galletti et al., 1999b) using single microelectrode penetrations with home-made glass-coated metal microelectrodes (tip impedance of 0.8-2MΩ at 1KHz) and multiple electrode penetrations using a 5 channel multielectrode recording minimatrix (Thomas Recording, GmbH, Giessen, Germany). The electrode signals were amplified (at a gain of 10,000) and filtered (bandpass between 0.5 and 5 kHz). Action potentials in each channel were isolated with a dual time-amplitude window discriminator (DDIS-1, Bak electronics, Mount Airy, MD, USA) or with a waveform discriminator (Multi Spike Detector, Alpha Omega Engineering, Nazareth, Israel). Spikes were sampled at 100 KHz and eye position was simultaneously recorded at 500 Hz with a Voss eyetracker. All neurons were assigned to area V6A following the criteria defined by Luppino *et al.* (2005) and described in detail in Gamberini *et al.* (2011).

### 3.3.2. Behavioral task

The monkey sat in a primate chair (Crist instruments) with its head fixed, in front of a personal computer-controlled rotating panel containing five different objects. The objects were presented to the animal one at a time, in a random order. During the inter-trial period, the panel was reconfigured by the computer to present a new object at the next trial in the same spatial position occupied by the previous object (22.5 cm away from the animal, in the midsagittal plane). The view of the remaining 4 objects was occluded. The same task has been used since we started this line of research in our lab (Fattori et al., 2010).

The reach-to-grasp movements were performed in the light and in the dark, in separate blocks. The Reach-to-grasp task is sketched in Fig. 5A and its time-course in Fig. 5B. In the dark condition (Fig. 5A, top) the animal was allowed to see the object to be grasped only for 0.5 s at the beginning of the trial, and then the grasping action was prepared and performed in the dark. In this way, the monkey was able to accomplish the reach-to-grasp movement adapting the grip to the object shape using a memory signal based on the visual information it had received at the beginning of each trial, well before the go signal. In the light condition (Fig. 5A, bottom), the two white LEDs illuminated a circular area (diameter 8 cm) centered on the object to be grasped, so

the monkey could see the object during the grasping preparation, and the object and its own hand during grasp execution and object holding.

The time sequence of the task is illustrated in fig 5B: the trial began when the monkey pressed the home button in complete darkness. After button pressing, the animal awaited instructions in darkness (*FREE*). It was free to look around and was not required to perform any eye or arm movement. After 1s, the fixation LED lit up green and the monkey had to wait for the LED change color (to red) without performing any eye or arm movement. After a fixation period of 0.5–1s, the two white lateral LEDs were turned on and the object was illuminated for a period of 0.5s (*OBJ-VIS*); the lights were then switched off for the rest of the trial in the dark (Fig. 5A, top). For the task in the light (Fig. 5A bottom), the lights stayed on for the rest of the trial (see “illumination light” line in Fig. 5B). After a delay period of 1-1.5s, during which the monkey was required to maintain fixation on the LED without releasing the home button (*DELAY*), the LED color changed. This was the go-signal for the monkey to release the button and perform a reach-to-grasp movement (*GRASP*) toward the object, to grasp it and to keep hold of it till the LED switched off (after 0.8-1.2s). The LED switch-off cued the monkey to release the object and to press the home-button again. Home-button pressing ended the trial, allowed the monkey to be rewarded, and started another trial (*FREE*) in which another object, randomly chosen, was presented.

In both task conditions, the monkey was required to look at the fixation point. If fixation was broken ( $5^{\circ}\times 5^{\circ}$  electronic window), trials were interrupted on-line and discarded. The correct performance of movements was monitored by pulses from microswitches (monopolar microswitches, RS Components, UK) mounted under the home button and the object. Button/object presses/releases were recorded with 1 ms resolution (see Kutz *et al.* (2005) for a detailed description of the control system of trial execution). In addition, the monkey’s arm movements were continuously video-monitored by means of miniature, infrared-illumination-sensitive videocameras.

#### 3.3.4. Tested objects

The objects and the grip types used for grasping are illustrated in Fig. 5C.

The objects were chosen such that they could evoke reach-to-grasp actions with different hand configurations.

*Handle*: thickness 2 mm, width 34 mm, depth 13 mm; gap dimensions: 28x11x2 mm. It was grasped with *finger prehension*, by inserting all the fingers (but not the thumb) into the gap.

*Stick-in-groove*: cylinder with base diameter of 10 mm and length of 11 mm, in a slot 12 mm wide, 15 mm deep and 30 mm long. It was grasped with the *advanced precision grip*, with the pulpar surface of the last phalanx of the index finger opposed to the pulpar surface of the last phalanx of the thumb.

*Ring*: external diameter: 17 mm; internal diameter: 12 mm. It was grasped with the *hook grip*, in which the index finger was inserted into the object.

*Plate*: thickness 4 mm, width 30 mm, length 14 mm. It was grasped with the *primitive precision grip*, using the thumb and the distal phalanges of the other fingers.

*Ball*: diameter: 30 mm. It was grasped with *whole-hand prehension*, with all the fingers wrapped around the object and with the palm in contact with it.

### 3.3.5. Data analysis

The analyses were performed with customized scripts in Matlab (Mathworks, Natick, USA, RRID SCR\_001622) and Python (using open source machine learning toolkit *scikit-learn*, <http://scikit-learn.org>, RRID SCR\_002577). The neural activity was analyzed by quantifying the discharge in each trial in four different epochs:

FREE: from button pressing to LED illumination.

OBJ-VIS: response to object presentation, from object illumination onset to illumination offset. This epoch lasted 500 ms.

DELAY: from the end of OBJ-VIS to movement onset. Epoch duration assumed random values between 1s and 1.5s.

GRASP: from movement onset (defined as the time of home button release) to movement end (defined as the time of object pulling). Movement period was not fixed over trials as it depended on the action execution time of the animal: Handle, 355.1ms; Stick-in-groove, 770.2ms; Ring, 421.7ms; Plate, 581.9ms; Ball, 576.1ms (average movement times).

We describe below the two types of analyses we performed on the data: *population response* and *neural decoding*.

All the analyses, neural information processing, and modeling were done offline.

### 3.3.6. Population response

We sequentially recorded 170 cells from two animals. We performed 3-way ANOVA (factor 1: epoch; FREE, OBJ-VIS, GRASP; factor 2: object/grip; 5 levels; factor 3, visual conditions; light/dark,  $p < 0.05$ ). In this study, we included the cells with significant main effects of epoch and object/grip in the decoding and population analyses. Among these cells, we considered only cells with 10 trials for each of the 5 objects, in each visual condition.

Population response was calculated as averaged Spike Density Function (SDF, see Fig. 6B). An SDF was calculated (Gaussian kernel, half-width 40ms) for each neuron included in the analysis, and averaged across all the trials for each tested grip. The neuron peak discharge found over all grip types during the GRASP epoch and during the OBJ-VIS epoch was used to normalize all SDFs for that neuron. The normalized SDFs were then averaged to obtain population responses (Marzocchi et al., 2008). Each condition was ranked and aligned twice in each plot, one based on the OBJ-VIS discharge (first alignment), and the other on GRASP discharge (second alignment).

### 3.3.7. Neural Decoding

Feature extraction and selection are crucial and challenging processes in machine learning. The goal is to select features that constitute a compact but informative representation of the phenomenon in order to analyze the neural coding in this study. For the purpose of our analysis, we assumed that neural information is coded as spike trains of firing neurons belonging to the same neural network. For each neuron of the population (79 neurons) we computed the Mean Firing Rate (mFR – number of spikes per time units) over a selected timespan using a trial-by-trial approach. The resulting feature vector thus consisted of the 79 mFRs of the entire neural population. Every trial was evaluated as a sample for the decoding algorithm. Thus, each trial, represented as a feature vector of 79 elements, was vertically concatenated with the other trials

to build the feature space. Since there were 10 trials for each of the 5 objects, the feature space was made up of 50 samples. The decoder outputs were the 5 objects or grip types. 5-fold cross-validation was performed by using 40 samples (8 for each condition) for training and 10 (2 for each condition) for testing for each neuron, so to ensure that the classifier was trained and tested on different data.

With the purpose of computing more robust and precise means of the classifier performance, we decided to computationally increase the number of test samples. Since neurons were recorded in separate sessions, and thus activity correlations between single neurons were already lost, we were able to expand the number of samples by shuffling the feature contributions of single neurons between trials, potentially obtaining  $10^{79}$  different vectors. We choose to randomly extend our dataset 10 times, thus performing our experiments on 400/100 training/test samples (100 per each of the 5 conditions), instead of the original 40/10. This procedure produced mean and standard deviation of object/grip classification accuracy based on firing rates. It is worth clarifying that artificially extending the dataset is not expected to improve classification accuracy, since no new information is added to the system, but it enables to compute a more precise mean given the few initial trials available. Non-normalized data were used for the decoding procedure.

We used a Naive Bayesian classifier as a neuro-decoder. Naive Bayes methods are a set of supervised learning algorithms based on applying Bayes' theorem with the "naive" assumption of independence between every pair of features. This technique has been shown to achieve performance closer to optimal compared to other classifiers when analyzing this kind of neural data (Scherberger et al., 2005; Townsend et al., 2011; Lehmann and Scherberger, 2013; Schaffelhofer et al., 2015). In our Python custom scripts we implemented the module of Naive Bayes classifiers proposed by *scikit-learn* libraries. The statistical formulation can be found here ([http://scikit-learn.org/stable/modules/naive\\_bayes.html](http://scikit-learn.org/stable/modules/naive_bayes.html), derived from Zhang, 2004). Under the assumption of Poisson distribution of features, we reinforced the model as suggested here ([github.com/scikit-learn/scikit-learn/pull/3708/files](https://github.com/scikit-learn/scikit-learn/pull/3708/files), Ma et al., 2006). To calculate the running time of the decoding algorithm, we used the *time* module embedded in Python.

We performed three types of analysis, computing the feature vectors over different epochs and timespans:

Whole epoch: mFR was computed over the whole OBJ-VIS, DELAY and GRASP epochs. Neuro-decoder predictions against real class, for each object or type of grip, are plotted as confusion matrices in Fig. 3.

Sliding window: mFR was computed over a window of 300ms which progressively slides over the reference period with a moving step of 10 ms (similarly to Carpaneto *et al.*, 2011). As in the previous case, training and testing sets were computed over the same time interval. This approach (Fig. 8) was used to see how the recognition rate changed dynamically over time.

Generalization analysis: mFR was computed over different intervals for training and testing sets: the system was trained over the whole OBJ-VIS and GRASP epochs and over four portions of the DELAY epoch; after having trained the system for an epoch, it was tested over all the epochs. This was done with the purpose of verifying whether the same code is used from object vision to movement execution, or alternatively trying to devise how the code changes during the delay epoch, before the movement and during movement execution. As the DELAY epoch varied in length from trial to trial, we performed the generalization analysis on 25% fractions of DELAY rather than on fixed size intervals.

In all experiments, classification performance was assessed by the rate of correct recognitions, and confusion matrices. These representations helped in understanding the most common error patterns of the classifier.

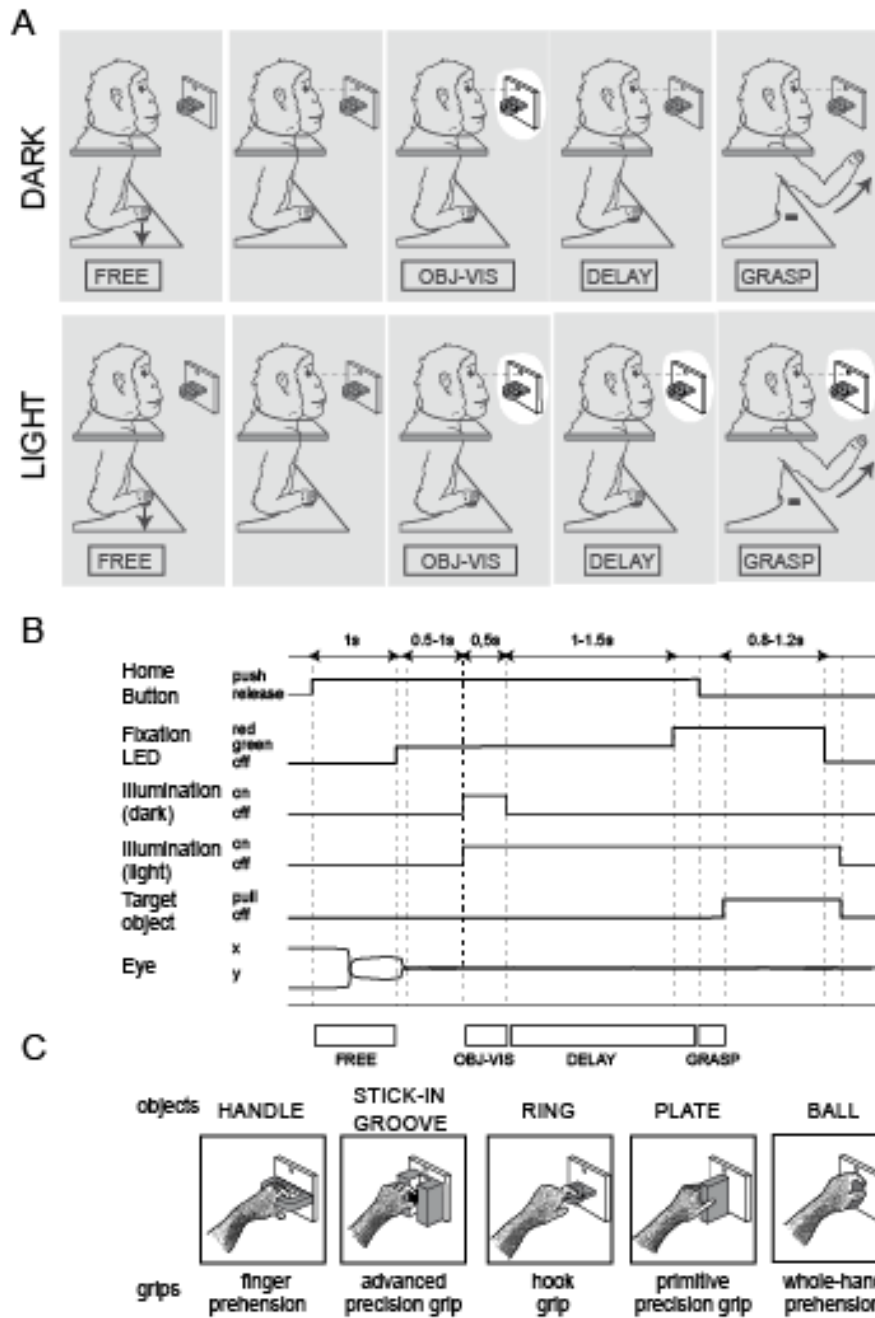


Figure 5. Reach-to-grasp task. A) Sequence of events in the Reach-to-grasp task in the dark (top) and in the light (bottom). The animal was trained to fixate at a constant location (fixation LED) shown as a small circle in front of the animal. It reached for and grasped an object (a ring, in this example) visible only in the OBJ-VIS epoch (dark condition) or in OBJ-VIS, DELAY, and GRASP epochs (light condition). In the dark, the Reach-to-Grasp action was executed in darkness, after a delay in darkness; in the light, the action preparation and execution were in the light with full vision of the object and of the hand interacting with the object. B) Time course of the Reach-to-Grasp task. The sequence of status of the home button, color of the fixation point (Fixation LED), status of the light illuminating the object (illumination), status of the target object (Target object, pulling and off) are shown. Below the scheme, typical examples of eye traces during a single trial and time epochs are shown. Dashed lines indicate task and behavioral markers: trial start (Home Button push), fixation target appearance (Fixation LED green), eye traces entering the fixation window, object illumination on and off (illumination on and illumination off, respectively), go signal for reach-to-grasp

execution (fixation LED red), start and end of the reach-to-grasp movement (Home Button release, and Target object pulling, respectively), go signal for return movement (fixation LED off), start of return movement to the home button (Target object off). C) Drawing (derived from videoframes) of the five objects and grip types used by the monkey. The object to be grasped changed from trial to trial, thus requiring different hand preshaping for the accomplishment of the grip. The orientation of the objects was chosen so that wrist orientation was similar in all cases. The five objects were grasped with five different grips: from the left, the handle with fingers only, the stick-in-groove with an advanced precision grip with precise index-finger/thumb opposition, the ring with the index finger only (hook grip), the plate with a primitive precision grip with fingers/thumb opposition, and the ball with the whole hand.

### 3.4. Results

Area V6A is known to contain grasp-related neurons (Fattori et al., 2004, 2009, 2010, 2012, 2017; Breveglieri et al., 2016). These cells are modulated by the different grip types required to grasp different objects and/or by the vision of the objects to be grasped. An example of one of these cells is shown in Fig. 6A. This cell fires when the monkey sees the object to be grasped and when the monkey plans and performs the reach-to-grasp action. These discharges are also different if the grasping was planned and executed in different visual conditions, the discharge being stronger in the light than in the dark (compare left with right columns). The visual discharge to object presentation (OBJ-VIS epoch) is tuned to the different objects, being strong for the ball and the plate, and maximal for the handle. Moreover, the motor-related discharges (GRASP epoch, G) are tuned to grasps occurring with different grips, from a maximum for grasping the handle to an almost null response for grasping the stick in groove.

Out of 170 V6A neurons recorded from 2 monkeys, 79 cells (47 from Case 1; 32 from Case 2) satisfied all the inclusion criteria (see Methods). The population discharge of the 79 grasp-related cells (3 way ANOVA,  $p < 0.05$ , see Methods) used for the decoding analysis is shown in Fig. 6B, where the activity of each neuron for each of the five tested objects was ranked in descending order to obtain the population response for the best (object or grip), the second best, and so on, up to the fifth, worst, grip. Each condition was ranked and aligned twice in each plot, one based on the OBJ-VIS discharge (first alignment), and the other on GRASP discharge (second alignment) for each individual background condition. The plot shows a clear distinction among the activations during the vision of the object, the preparation and the execution of reach-to-grasp actions. Moreover, Fig 6B shows that the V6A neural population starts discriminating between different objects/grips as soon as the object becomes visible to the animal (OBJ-VIS). The discrimination

power of the population remains constant when the monkey is preparing the action (DELAY), and has a second peak when the action is executed (GRASP), as the huge difference between best (red line) and worst (blue line) responses shows. This trend is common to population activity in the dark and in the light.

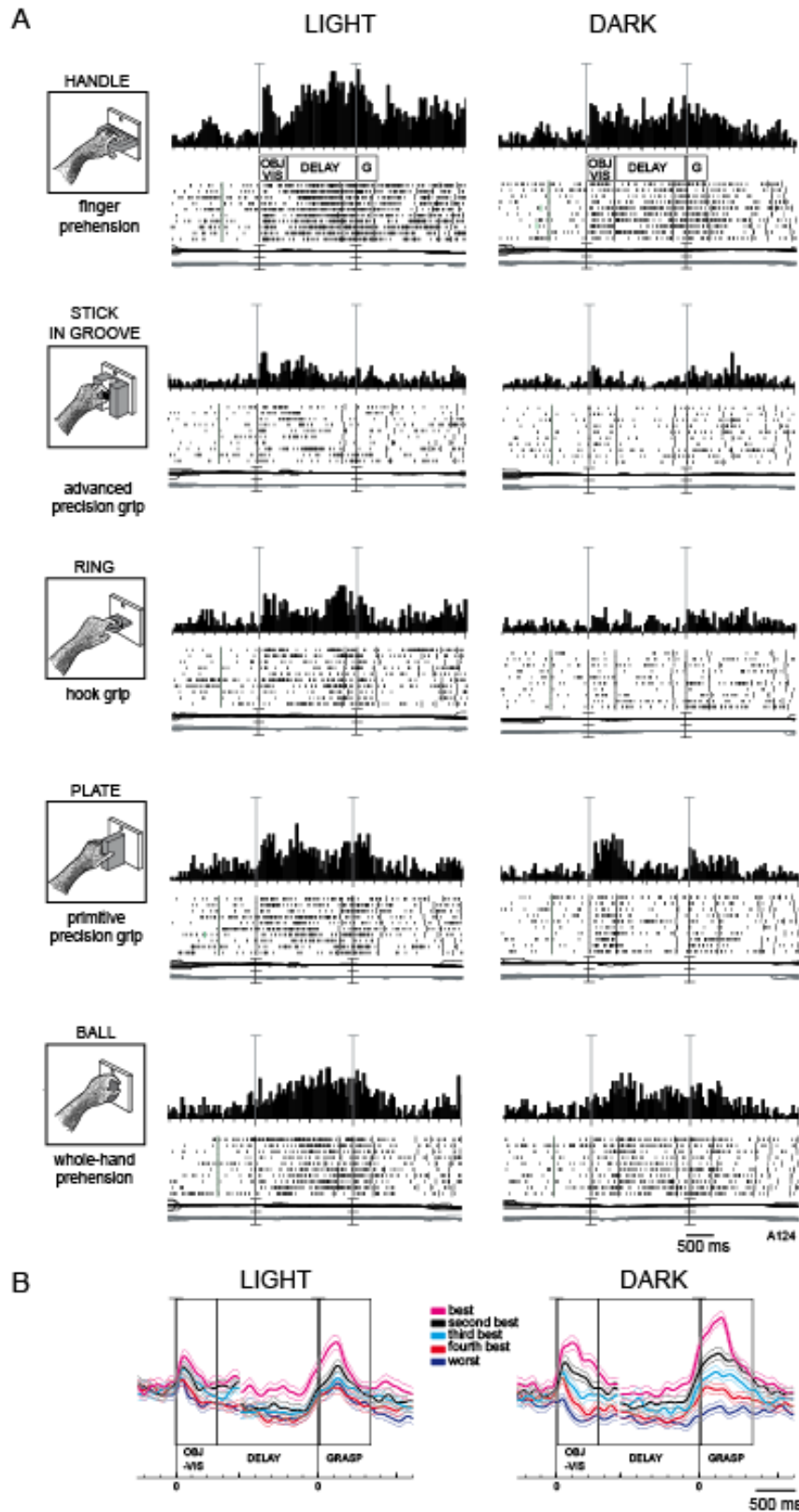


Figure 6. Object and grip selectivity in V6A. A) An example of a V6A neuron selective for object and for grip type and influenced by the vision of the object and of the action. Left: objects and types of grips. Right: activity is illustrated as peristimulus time histograms (PSTHs) and raster displays of impulse activity, left in the light and right in the dark. Below each discharge there is a record of horizontal (upper trace) and

vertical components (lower trace) of eye movements. Neural activity and eye traces are aligned (long vertical line) twice, on object illumination onset and on movement onset. Long vertical ticks in raster displays are behavioral markers, as indicated in Fig. 1B. Rectangles under the PSTH of the first object represent the duration of epochs (G=GRASP). The cell displays selectivity for the task conditions during the times of object presentation, delay and the execution of grasp action. Vertical scale on histogram: 76 spikes/s; time scale: 1 tick=200ms. Eye traces: 60°/division. B) Population data. Activity of 79 grip-selective V6A neurons used for the decoding procedure expressed as averaged normalized SDFs (thick lines) with variability bands (light lines), constructed by ranking the response of each neuron for each individual object according to the intensity of the response elicited in the OBJ-VIS epoch (left, activities aligned with the onset of the object illumination) and according to the intensity of the response elicited in the GRASP epoch (right, activities aligned with the onset of the reach-to-grasp movement) in descending order (from magenta to blue). In other words, each condition was ranked and aligned twice in each plot, one based on the OBJ-VIS discharge (first alignment), and the other on the GRASP discharge (second alignment). The SDFs of each alignment were calculated on the same population of cells. Each cell of the population was taken into account five times, once for each object/grip. Scale on abscissa: 200ms/division (tick); vertical scale: 80% of normalized activity.

### 3.4.1. Decoding results

The neural activity of 79 grasp-related V6A neurons was analyzed offline in three main epochs: OBJ-VIS, DELAY, and GRASP, corresponding to the period of visual stimulation provided by the object, the planning phase of the subsequent reach-to-grasp action and the execution phase, respectively. It is worth remembering that, in the dark condition, the animal was in darkness during DELAY and GRASP (except for the fixation LED), whereas in the light condition the animal prepared and executed the grasping action in the light, thus with the availability of visual information on the object and its hand/arm approaching and interacting with the object. The results, obtained from two cases, were similar for individual animals. Thus, the results of the two cases are presented jointly.

Although we performed decoding off-line, having in mind a future possible application of this methodology in a real-time loop, we calculated the running time of the decoding algorithm. Since in this setting only the prediction phase is relevant, we parsed the time required to run that phase only, given the already trained classifier. We found that the running time was extremely short, with a mean required time of 0.26 ms (sd 0.04), calculated on 100 iterations.

### 3.4.2. Object recognition within the object presentation epoch

The decoding results of the time span in which the object was illuminated in both visual conditions (OBJ-VIS epoch) are presented in Fig. 7AB. Using a Naïve Bayes classifier as neuro-decoder (see Materials and Methods), we found a high correlation between the actual conditions and the decoded conditions, as illustrated in the confusion matrices. The mean accuracy, obtained using leave-p-out cross-validation testing over 20% of trials, was lower in the decoding in dark than in light conditions: in the dark, the mean accuracy was 81.6%, whereas in the light it was 91.8% (+/- 0.8%). However, the decoding performance in the dark is highly variant (standard deviation=12%), whereas in the light the variance is almost null (standard deviation=0.8%). The apparently odd difference in performance in OBJ-VIS, where the visual conditions are identical, and the high variance in the dark can be explained by the presence of other factors influencing the discharge during OBJ-VIS. We suggest that the attentional level of the monkeys is higher in the dark than in the light (where the monkeys know that the visual information of the object will be available until the end of the trial), and this can add noise to the system, causing a decrease and a higher variance in decoding performance.

Considering each animal separately, the performance slightly decreases in the light as well as in the dark, although in both individual cases the level remained well above chance (see Table 1).

	OBJ-VIS		DELAY		GRASP	
	Dark	Light	Dark	Light	Dark	Light
<b>Cases 1+2</b>	81.6 +/-12%	91.8 +/- 0.8%	97.2+/2.9%,	100 +/-0.0%,	98.4 +/-2.1%	100+/-0.0%
<b>Case 1</b>	67.6 +/-10.2%	78.6 +/-10.4%	81.6 +/-11%	98.8 +/-0.9%	91.4 +/-2.7%	98 +/- 0.4%
<b>Case 2</b>	74.4 +/-12.7%	68.6 +/-10.5%	86.8 +/-3.7%	93.6 +/-5%	84.6 +/-4.3%	96.2 +/-3.7%

Table 1. Performance, expressed as mean accuracy +/- standard deviation, of the classifier in the two cases (together and separated).

## CONFUSION MATRICES

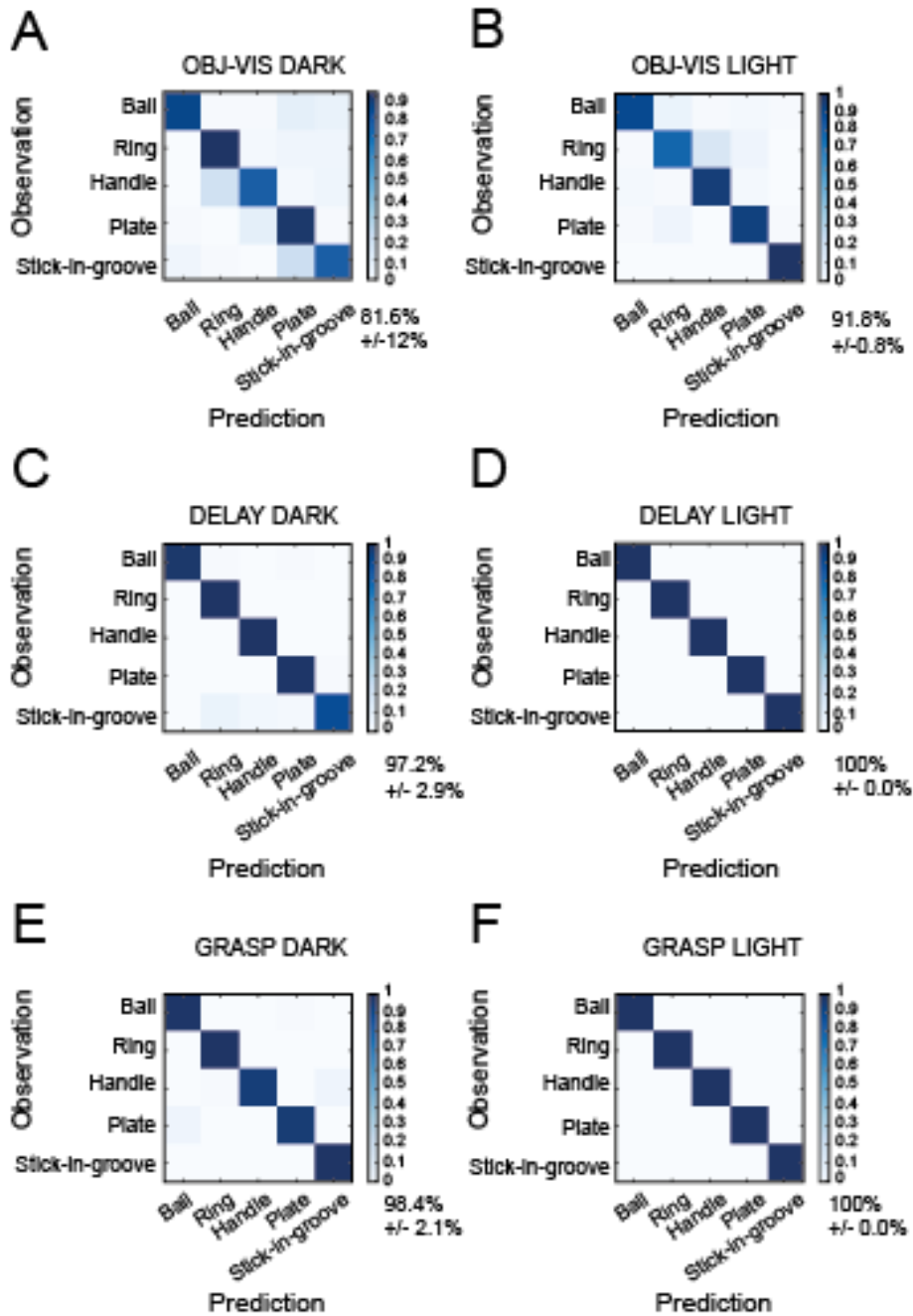


Figure 7. Confusion matrices describing the pattern of errors made by the Naïve Bayes classifier in the recognition of tested objects or grip types. Mean firing rates were calculated for different epochs (A-B, OBJ-VIS; C-D, DELAY; E-F GRASP) and conditions (DARK left, and LIGHT right). The matrices summarize the results of cross-validation iterations plotted as real class (observation) against predicted class (prediction). Contributions of 79 neurons from V6A area were included in the dataset for the decoding analysis. Blue color scale indicates the accuracy yield by the algorithm as reported in the side indices, mean recognition rates are reported together with standard deviations below the indices.

### 3.4.3. Time-course of the decoding performance

Although confusion matrices are very informative about the decoding performance, they do not provide any insight on the temporal dimension. To fill this gap, we estimated the time course of the classifier performance by computing firing rates in time intervals around light and movement onset. Fig. 8AB shows the classification performance in the dark and in the light, respectively, when the feature was extracted from a time window of 300 ms, which progressively slides over the trial timespan from 500 ms before illumination onset to 1 second after the movement onset, with a moving step of 10 ms. We employed a double alignment because of the variability in the delay duration.

In the dark and in the light, the time course of the recognition rates was slightly different. In the dark (fig. 8A) there was a quick increase of the decoding performance, up to 80% occurring after the illumination onset related to the object's vision. About 600 ms after the illumination onset (that corresponds to 100 ms after the switch-off of the object illumination), the recognition rate decreased to about 75%, and this performance remained constant in the subsequent delay and slightly increased at the end of the delay. In the light (fig. 8B), the accuracy was higher than in the dark during object observation, whereas in the delay it was similar to the dark condition. However, the recognition rate increased more pronouncedly during the last part of the delay (see the curve in the right part of Fig. 8B before the second alignment). During grasp execution, the recognition rate was particularly high, especially in the light, and remained high till the end of grasp execution. To summarize, we found a ramp-up trend of the decoding performance in both conditions. After object illumination, the accuracy increased with time as movement onset approached, reaching maximum values at the end of the delay period, particularly in the light. We can reliably say that the accuracy reaches the maximum value when the hand is approaching the object, better if the animal is able to see the action.

## SLIDING WINDOW ANALYSIS

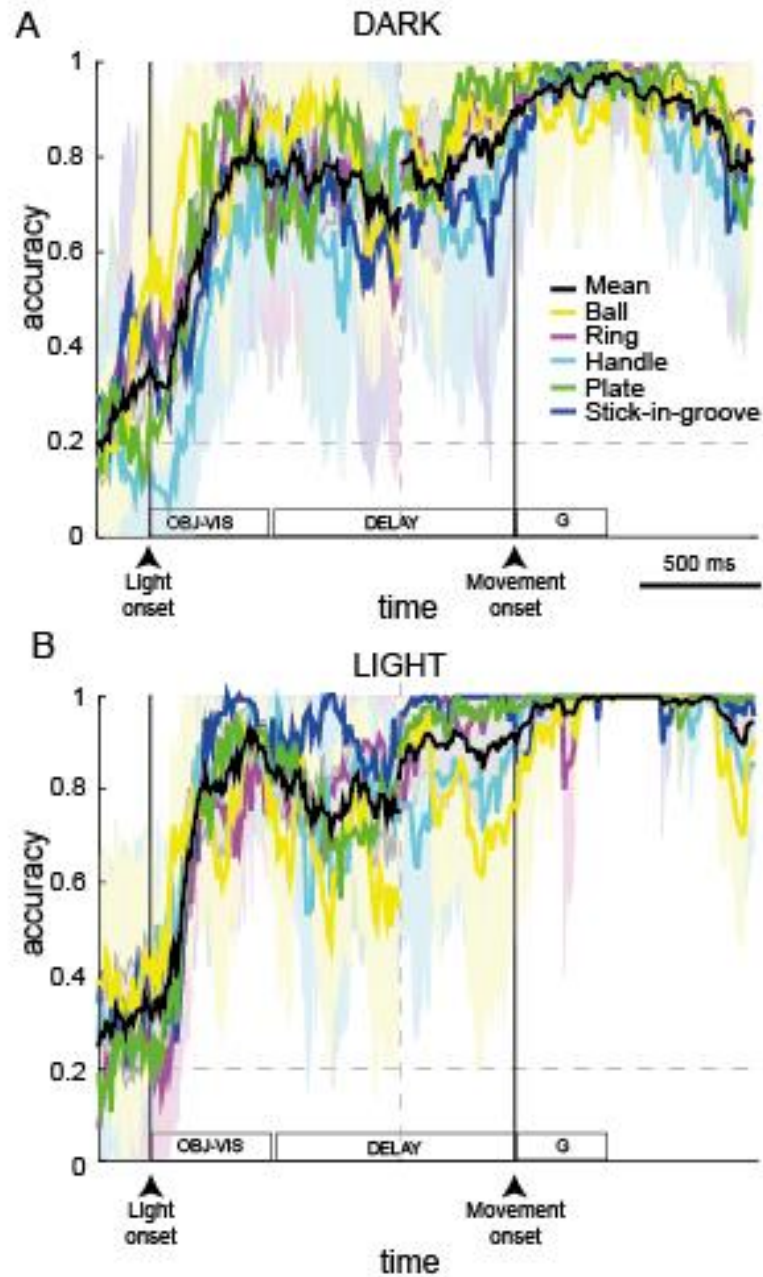


Figure 8. Sliding window analysis. Time course of the decoding accuracy (recognition rates) based on the firing rates extracted during the period starting 500ms before the light onset, through 1s after the movement onset. Due to the variable duration of the delay (1-1.5s), double alignment result plots are shown. The first alignment coincides with the object illumination onset, the second one with the movement onset. Firing rates were calculated for a 300ms sliding window, moving forward with a 10ms step. Each dot on the graphs was plotted at the beginning of each 300ms window. The mean line (black) was calculated as the arithmetic mean between recognition rates of individual objects (colored lines). For each object, variability bands are shown, representing standard deviations based on 5-fold cross-validation.

#### 3.4.4. Generalization analysis

To evaluate whether the neural code used during object observation was retained or changed during the subsequent delay before the grasping onset, we performed a generalization analysis by training classifiers either in OBJ-VIS or in GRASP, and we applied both codes on portions of the DELAY epoch. Fig. 9 shows the results of this analysis in the dark (Fig. 9AC) and the light (Fig. 9BD). The performance of the decoding algorithm trained using the neural activity during OBJ-VIS is indicated in blue (Fig. 9AB). The performance using GRASP activity is shown in red (Fig.9AB). The performance using DELAY portions is shown in greyscale (Fig. 9CD). In the dark, the code learned during OBJ-VIS and generalized during DELAY gave much lower accuracy (fig 9A, blue line). The accuracy subsequently dropped to much lower values (around 40%) during movement execution. This suggests that the neural code employed during object observation quickly became weaker as soon as the animal began to prepare the movement. In the light, the accuracy obtained by training the algorithm using the OBJ-VIS epoch and tested on the DELAY fractions (fig 9B, blue line) was almost as high as during the vision of the object, so the same code was maintained during the DELAY in the light. This is likely because the visual information regarding the object was still available in the delay of the light condition. Again, as seen for the dark, the decoding performance dropped to about 40% during grasp execution.

In the dark, the time-course of the accuracy obtained by training the algorithm with the GRASP neural activity (Fig. 9A, red curve) and tested in the DELAY demonstrated that the neural code used during action execution was partially present also during the last fraction of the delay, but dropped abruptly immediately before it. So, the same code seems not applicable during object observation (OBJ-VIS) and during the first parts of the DELAY. In the light (fig 9B, red line), on the other hand, the code obtained by decoding from GRASP dropped gradually during the DELAY: a decreasing trend of accuracy is apparent throughout the DELAY.

When analyzing the accuracy of the classifier trained in the different fractions of the DELAY (grey lines in Fig. 9 CD), code similarities are highlighted. In the dark, a noticeable difference between the first part of the delay (lighter grey) and the subsequent fractions (darker greys) is evident: the late codes share similarities, whereas the initial code is quite different. This highlights that, after object disappearance, there is a gradual transformation of the code from object observation to motor execution. On the other hand, in the light, the code, presumably related to visual information, was maintained longer, probably thanks to the availability of visual information.

Overall, in the light, code differences were minimized, conceivably because information collected was more similar through portions of the DELAY.

To summarize, different codes were present from object observation to movement execution, but their relative influence on the overall neural activity varied over time. In both visual conditions there was a switch between the codes during the last parts of the delay. Moreover, this analysis shows that the neural population during the DELAY epoch switched its preferential coding feature, and this likely suggested that a transformation from visual information into motor representation was performed at that time and encoded by these neurons. In this study, in the five task conditions, each of the different objects was grasped with a clearly distinct grip. Therefore, selectivity for object and for grip type is necessarily strongly correlated and cannot be distinguished in our task. So, the change of coding observed in the generalization analysis does not necessarily imply a change of representation, i.e., from a code representing objects to one representing grip type. However, a possible explanation is that the decoded discharge from V6A reflects the visuo-to-motor transformations occurring in the DELAY period in which the visual information regarding the object (visual/object coding) is transformed into motor commands (motor/grip coding).

## GENERALIZATION ANALYSIS

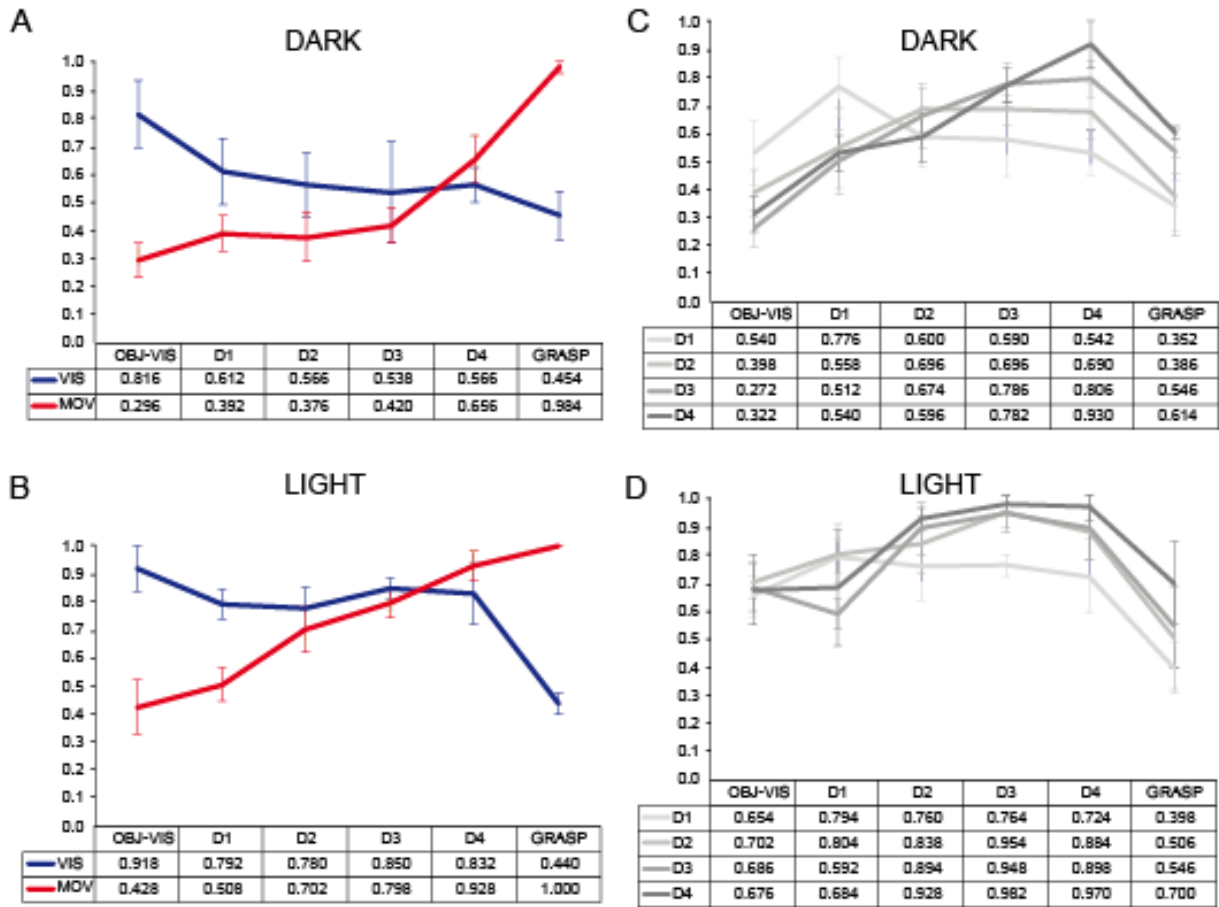


Figure 9. Generalization analysis. Generalization of codes derived from different epochs for dark (A, C) and light (B, D) conditions. The neuro-decoder trained with the firing rates extracted from one epoch was used to decode all epochs. The trend of mean recognition rates together with the standard deviation bars through different epochs are plotted as coloured lines: in A and B, red= the classifier was trained on OBJ-VIS; blue=the classifier was trained on GRASP; in C, D, greyscale= the classifier was trained on fractions of the DELAY epoch. The DELAY epoch was split in portions due to variable time duration between the trials: D1= 0-25% of the DELAY epoch; D2= 25-50%; D3=50-75%; D4=75-100%. The accuracy obtained from the activity of each time interval is shown under each plot.

### 3.5. Discussion

The above experimental results show that the posterior parietal area V6A of the dorsomedial visual stream represents a reliable site for decoding information for grasping in the presence and in the absence of visual information regarding object and hand/object interaction available when the action is prepared and executed. This opens new perspectives and possibilities about the source of grasp-related signals that may be used to implement BCIs.

In our experiment, each tested object was grasped with a clearly distinct grip. In these conditions, selectivity for object shape and for grip type cannot be distinguished, unlike other studies (e.g. Schaffelhofer and Scherberger, 2016) where more objects and a larger variability of grip types were tested. Although an inherent decoding ambiguity cannot be avoided in our study, good decoding results have been achieved from a restricted number of grasp-related neurons from V6A, in accordance with what was found in PMv by Carpaneto and colleagues (Carpaneto et al., 2011), and PPC itself, for decoding reach trajectories (Aflalo et al., 2015). In addition, the number of trials, 10 in our case, is low for decoding; despite this, we still obtained an extremely high classification accuracy.

We found high recognition rates in different time epochs: the visual presentation of the object (OBJ-VIS), the delay before the movement (DELAY), and the period of reach-to-grasp execution (GRASP). In addition, the different visual conditions used show that combining visual and motor information could slightly modulate the power of the classification.

A very good recognition rate was obtained during the vision of the object well before grasping execution. This could indicate the presence in V6A of covert motor commands for the upcoming grasp, because animals were overtrained to grasp the objects used in this task. However, we are more inclined to suggest that the encoding occurring during the vision of the object reflects object recognition for action, as already shown for V6A in a work where visual responses to objects with different shapes evoking different grips were demonstrated to reflect object affordance (Breveglieri et al., 2015). The slightly higher accuracy obtained during movement execution in the light compared with the dark is suggestive of a weak effect of the vision of hand-object interaction in V6A.

The delay period between object presentation and grasp execution proved to be a good source of decoding in V6A (see Fig. 5 CD). Generalization analysis showed that in the first part of the delay, spanning some hundreds of milliseconds after the end of object illumination, well beyond transient visual responses (Thorpe et al., 1996; Schmolesky et al., 1998), the decoding was mostly effective if performed through an OBJ-VIS epoch derived code, likely representing a *visual/object* code (see Fig. 9). This epoch is followed by an intermediate visuo-motor transformation stage, in which the brain likely converts the visual information into motor commands. Here we illustrated that decoding from V6A is still possible, but with a lower accuracy. Then, in the third part of the delay, we can obtain a higher decoding accuracy than the two first intervals. In this last phase, the decoding is most successful when using a GRASP derived code, possibly representing a *motor/grip* code. This last period, close to motor execution, but well in advance with respect to possible afferent feedback signals (known to be present in V6A, see Breveglieri *et al.* 2002; Fattori *et al.* 2005; 2015), could reflect an efferent command or an action plan where planned grasp coding information is present. These results from the performance of the neuro-decoder parallel those found simply by analyzing mean frequencies of discharge in this same area: in V6A there is an encoding of the visual attributes of objects at the beginning of the DELAY period that switches to a grip type encoding during the DELAY period, when the prehension action is planned, and later during movement execution (see Fig.8 Fattori et al., 2012). For the purpose of decoding, at first glance, the coexistence of different coding schemes can be seen as a disadvantage, due to the lack of a clear distinction between employed codes and the resulting increase in the data complexity. Potentially, however, properly trained multiple decoders can efficiently recover visual and motor attributes from the same dataset. Conceivably with the aid of a post processing algorithm, the decoder results can be integrated together in order to obtain more accuracy and/or additional data for a visuomotor guided robotic prosthetic arm.

This anticipated decoding ability seems to be typical of the parietal cortex (see Andersen *et al.* 2010) where the reaching goals and trajectories were decoded 190 ms after target presentation (Aflalo et al., 2015), thus comparable with V6A for grasping decoding (Fig. 4A). Precocious decoding from PPC would allow signals to be sent to the computer interfaces well before the movement needs to be initiated. Together with the short time required to run the classifier algorithm (a few tenths of a millisecond for the prediction phase, in our work), this fits well with a real time decoding implementation.

### 3.5.1. Offline decoding from single cells in dorso-medial fronto-parietal areas: perspectives on BCIs

In this study, as in some others in the dorsolateral visual stream (see also Carpaneto *et al.* 2011; Townsend *et al.* 2011), the neural decoding with a high accuracy for grasping was performed offline from single cells, thus confirming that this kind of signal is adequate to be exploited for successful decoding. In addition, this work adds a novel area in the panorama of the brain areas useful for BCIs. So far, all the studies aimed at decoding grasps used signals from the primary motor cortex (Carpena *et al.*, 2003; Hochberg *et al.*, 2006, 2012; Kim *et al.*, 2006; Ben Hamed *et al.*, 2007; Velliste *et al.*, 2008; Vargas-Irwin *et al.*, 2010) or the dorsolateral fronto-parietal network, specifically the lateral premotor area F5 (Carpaneto *et al.*, 2011, 2012; Townsend *et al.*, 2011; Schaffelhofer *et al.*, 2015) and the lateral posterior parietal area AIP (Townsend *et al.*, 2011; Klaes *et al.*, 2015; Schaffelhofer *et al.*, 2015).

In area AIP, the best performance was achieved during the reach to grasp task in the Cue epoch (Schaffelhofer *et al.*, 2015). Conversely, in V6A, the best performance occurs in the GRASP epoch. This feature is similar to area F5, where the best performance was obtained during grasping execution (Carpaneto *et al.*, 2011; Schaffelhofer *et al.*, 2015), especially in the light. These results suggest that, although areas V6A and AIP are both grasp-related parietal areas which share many functional properties (see also Breveglieri *et al.* 2016), AIP seems to be more involved during the vision of the object and V6A during movement execution.

Recently, Andersen's lab decoded visual and motor aspects of complex hand shaping from human area AIP (Klaes *et al.*, 2015). Decoding of grasp information from monkey's AIP is well supported (Townsend *et al.*, 2011; Schaffelhofer *et al.*, 2015), and these very recent data on human AIP suggest a good functional affinity between monkeys and human PPC. The present data on decoding of objects and grasps from this other parietal site promises a future for decoding grasps from human dorsomedial parietal cortex.

Indeed, so far, decoding neural signals from dorsomedial areas has been done in the context of reconstructing hand position in space (Hatsopoulos *et al.*, 2004), or finger flexion/extension movements (Aggarwal *et al.*, 2009) and reach trajectories (Musallam *et al.*, 2004; Mulliken *et al.*, 2008a; Hwang and Andersen, 2013; Aflalo *et al.*, 2015). This is the first work in which an area of

the dorsomedial visual stream is used successfully to decode grasps. It encourages researchers to look at other dorsomedial stream areas involved in grasping, such as PMd (Raos et al., 2004; Stark et al., 2007), as possible targets of decoding for prehensile actions.

### 3.5.2. Future directions

Since the first demonstrations of monkey medial PPC as a site encoding intentions for reaches (Snyder et al., 1997), attention has been given to this region as a site useful for translating basic research on monkey neural recordings into applications useful for BCIs (Musallam et al., 2004; Mulliken et al., 2008a). Recent evidence shows that non-human primate and human PPC share a similar sensorimotor function (Aflalo et al., 2015; Klaes et al., 2015). In fact, by recording from the PPC of tetraplegic subjects, Andersen and coworkers showed that neural signals from human medial PPC may be used for BCIs to guide reaching movements to appropriate goals with appropriate trajectories (Aflalo et al., 2015) and from lateral PPC to control hand shaping (Klaes et al., 2015). The present results indicate that monkey *medial* PPC hosts neural signals that could be used to implement BCIs to guide prehensile actions to grasp objects of different shapes with different grips. Future studies might obtain similar advantages by applying the decoding algorithms to neural signals from human medial PPC to control signals in assistive devices for impaired patients (tetraplegics or subjects affected by neurodegenerative diseases that impair hand functions). This might be useful in recovering full control of a hand.

## 4. Prediction of reach goals in depth and direction from the parietal cortex

MATTEO FILIPPINI<sup>1</sup>, ROSSELLA BREVEGLIERI<sup>1</sup>, KOSTAS HADJIDIMITRAKIS<sup>1,2,3</sup>, ANNALISA BOSCO<sup>1</sup>, PATRIZIA FATTORI<sup>1</sup>;

<sup>1</sup>University of Bologna - Department of Biomedical and Neuromotor Sciences, Bologna, Italy; <sup>2</sup>Biomedicine Discovery Institute and Department of Physiology, Monash University, Clayton, Victoria 3800, Australia. <sup>3</sup>Australian Research Council, Centre of Excellence for Integrative Brain Function, Monash University Node, Clayton, Victoria 3800, Australia.

### 4.1. Summary

The posterior parietal cortex is well known to mediate sensorimotor transformations during the generation of movement plans, but its ability to control prosthetic limbs in 3D environments has not yet been fully demonstrated. With this aim, we trained monkeys to perform reaches to targets located at various depths and directions and tested whether the reach goal position can be extracted from parietal signals. The reach goal location was reliably decoded with accuracy close to optimal (>90%) and this occurred also well before the movement onset. These results, together with recent work showing a reliable decoding of hand grip in the same area, suggest that this is a suitable site to decode the entire prehension action, to be considered in the development of new brain computer interfaces.

## 4.2. Introduction

When a spinal cord injury or other diseases do not allow motor commands to reach the muscles, the patient is unable to perform voluntary actions, despite an intact brain. In cases like these, the advent of Brain Computer Interfaces (BCIs) has offered a possibility to gain control of external devices (neural prostheses) by using the patient's own brain activity (Brandman et al., 2017). Although in the last decade several technical advances provided impressive examples of successful human applications, the performances achieved are still far from enabling widespread clinical application (Cui, 2016). So far, the majority of studies have used primary motor and premotor cortex signals to reconstruct reach trajectories in order to guide robotic limbs in monkeys (Wessberg et al., 2000; Velliste et al., 2008) and humans (Hochberg et al., 2012; Collinger et al., 2013). Although decoding of trajectories is still essential in order to provide the user with natural interfaces, progress in computer vision and robotics is leading to prostheses that do not require trajectory information, as simple algorithms can reconstruct this information from reach endpoint goals (Andersen et al., 2014; Katyal et al., 2014; Hotson et al., 2016).

The posterior parietal cortex (PPC) in humans and monkeys is involved in the sensorimotor transformations required to generate action plans (Andersen et al., 2014; Cui, 2016; Gardner, 2017), so it is a good source for retrieving movement intentions and goals. Pioneering studies demonstrated that reach endpoints (Serruya et al., 2003; Musallam et al., 2004), trajectories (Mulliken et al., 2008, Fig. 10A), and grips (Schaffelhofer et al., 2015, Fig. 10A) can be extracted from monkey PPC. Translational work in humans gave similar results (Aflalo et al., 2015, Fig. 10B), together with reliable hand shape decoding (Klaes et al., 2015, Fig. 10B). In the aforementioned studies, reaches were performed on a single plane. To the best of our knowledge, only one study in monkey PPC performed decoding of reach goal and trajectory information in a virtual 3D environment (Hauschild et al., 2012).

A medial PPC area termed V6A (Fig. 1A) is known to encode not only goals and reach movement directions (Bosco et al., 2010, 2016; Breveglieri et al., 2014; Hadjidimitrakis et al., 2014a), but also several grasping parameters (Fattori et al., 2017). Previous research suggested that V6A could integrate the arm transport and hand grip components of a reach-to-grasp action. (Galletti and Fattori, 2018). While a reliable decoding of hand grip from V6A signals has recently been shown (Filippini et al., 2017), decoding of reach-related information has not yet been performed (Fig. 1A). We addressed this issue, with the aim of finding a parietal region where both grasping and

reaching signals can be decoded. In a different way to most previous related studies, we varied reaches not only on a frontoparallel plane, but using a naturalistic environment also involving depth (distance from the body).

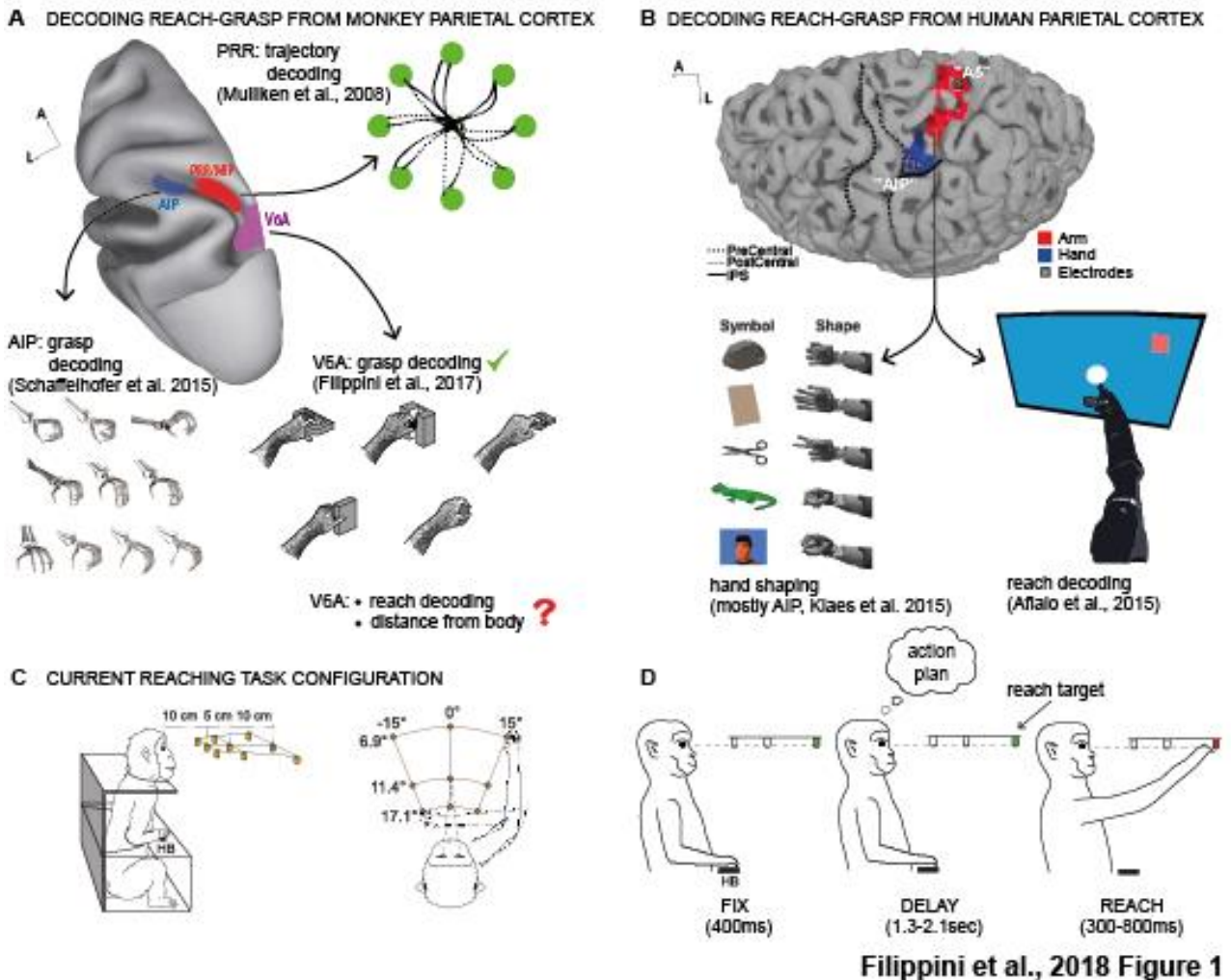


**Figure 10.** A. Decoding for reaching and grasping by the monkey posterior parietal cortex. Top left: Dorsal view of the left hemisphere of a macaque brain. Highlighted hot spots in the parietal cortex represent areas used in recent literature to extract signals useful to decode grasp (area AIP, anterior intraparietal area from Schaffelhofer et al., 2015) and/or movement trajectories (PRR –parietal reach region-MIP, medial intraparietal area, from Mulliken et al., 2008). V6A signals have recently been used to decode grasping (Filippini et al., 2017). The goal of the present study was to decode reaching targets by the V6A. A, anterior; L, lateral. B. Decoding in the human posterior parietal cortex for reach on a frontal plane (Aflalo et al., 2015) and hand shapes (Klaes et al., 2015) separately. A5, Brodmann’s area 5; modified from Aflalo et al (2015) and Klaes et al (2015). C. Scheme of the setup used for the task in the present study. Left: nine light-emitting diodes (LEDs) that were used as fixation and reaching targets (orange) were located at eye level. The distances from the eyes of the 3 targets of the central row are shown. HB, home button. Right: top view of the target configuration showing the values of version (top) and vergence angles (left). Targets in different positions on the horizontal axis have a different laterality (direction); on the horizontal axis, targets change in distance from the body (depth). D. Cartoon of the fixation-to-reach task performed by monkeys. Left: in the first part of the task (FIX epoch), the monkey had to fixate one of 9 targets. In the DELAY epoch (center) the monkey had to maintain fixation on the target and wait for the go signal (i.e.

target color changing from green to red) while planning the action. Right: REACH, the monkey released the home button to perform the reaching movement toward the target.

### 4.3. Results

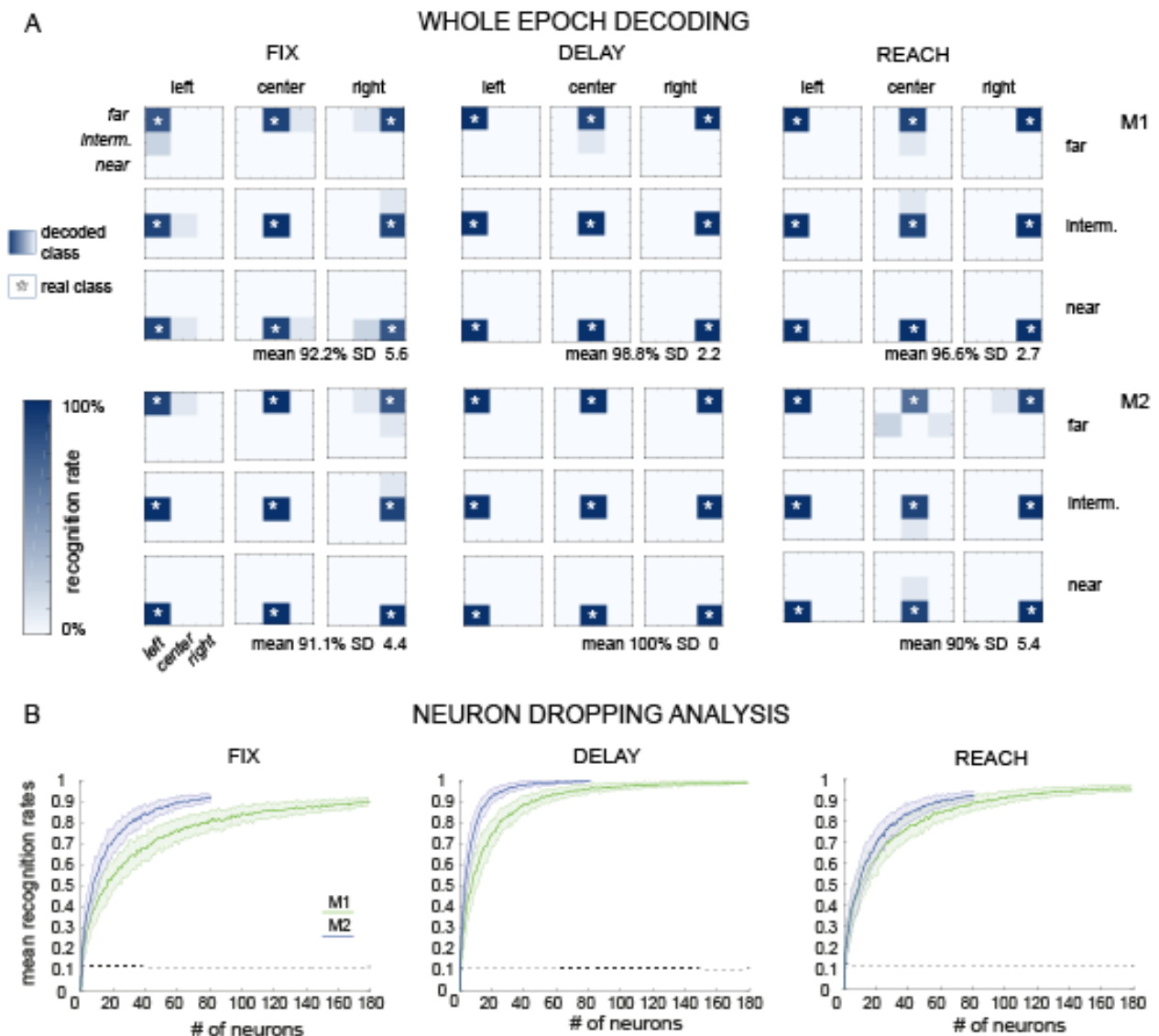
Data were recorded from two monkeys while they performed a Fixation-to-reach task toward nine spatial positions with three different direction angles and three different depth levels (see Fig. 10C), covering a wide range of positions in peripersonal space. Target elevation was kept constant, at eye level. We sequentially recorded 264 V6A cells, 181 neurons in monkey 1 (M1) and 83 in monkey 2 (M2). Parts of this dataset have already been published in previous studies aimed at exploring the encoding of depth and direction in V6A activity (Hadjidimitrakis et al., 2014a, 2017). The population discharge of the whole dataset is shown in Fig. S1A. The plot shows a clear distinction among the activations during the early vision of the target, then during the preparation and finally during the execution of reaching action. Moreover, Figure S1A shows that the V6A neural population starts discriminating among different targets as soon as the LED is illuminated. The discrimination power of the population increases slightly when the monkey is preparing the action (epoch DELAY, from 450 ms after the fixation onset to the arm movement onset), and has a second peak when the action is executed (REACH). Population tuning properties were confirmed by a sliding window ANOVA (Figure S1B).

**4.3.1. Whole epoch decoding.** The activity of each neuron was quantified in the three main epochs depicted in Fig. 10D: FIX, DELAY and REACH, corresponding to the period of early fixation of the target, the planning phase of the subsequent reach action and the execution phase, respectively. Subsequently, population decoding analysis was performed using a naive Bayes classifier (see Experimental Procedures). The results are presented separately for the two monkeys. In each monkey, all recorded cells were included in the analysis, irrespectively of whether they responded differently depending on the position of the target or not.

Our decoder correctly classified target positions well before movement onset: we found a high correlation between the actual and the decoded spatial positions during FIX (Fig. 11A). The mean accuracies, obtained using a 'leave-p-out' fivefold cross-validation (p value 20% of trials), were excellent in both monkeys (91-92%) and well above chance level (11%, the conditions being 9).

Misclassifications were very few and occurred between adjacent targets. The decoding accuracies during both reach planning (DELAY) and execution (REACH) were even higher than during FIX, again in both monkeys.

4.3.2. Neuron Dropping Analysis. Figure 11B depicts the decoding accuracy as a function of the population size. Results varied across epochs and monkeys: in FIX (Fig. 11B, left), a sample of 20 to 40 neurons (median: 40) was sufficient to achieve 70% accuracy, whereas in REACH (Fig. 11B center), 20-30 neurons (median: 26) and DELAY (Fig. 11B right), between 10 and 20 neurons (median: 15) were required. In all cases, a small number of neurons was enough to obtain accurate decoding.



Filippini et al., 2018 Figure 2

**Figure 11.** A. Whole epoch decoding. Confusion matrices describing the pattern of errors made by the naïve Bayes classifier in the recognition of target positions. Mean firing rates were calculated for different epochs (left, FIX; center, DELAY; right, REACH) and monkeys (first row, monkey 1 (M1), middle row, monkey 2 (M2)). In each 3x3 sub-matrix, the actual goal location is indicated as a white asterisk according to its position in the monkey's workspace (near/intermediate/far and left/central/right). For each real class, decoder predictions (recognition rate) were plotted with a color scale. Mean recognition rates are reported together with SDs (standard deviations) below the indices. These matrices show the highly successful decoding and that the few not perfect classifications involve spatially close target positions.

B. Neuron Dropping Analysis. Accuracy of decoding as a function of the number of neurons included in the analysis. Dotted line, chance level (0.11). For each step (0 to neurons available per monkey), we randomly caught an increasing number of neurons from the pool, to include in the analysis. This procedure was repeated 100 times per step to calculate SD values. Results are shown for the two cases (green, M1; blue, M2) and the three epochs analyzed. All in all, it is evident that a maximum of 20-40 neurons is required to efficiently decode reach goals.

**4.3.3. Time course of the decoding performance.** To evaluate the temporal evolution of decoding accuracy, we estimated the decoding performance using activity in smaller time intervals compared to the whole epochs. A rapid increase of the decoding performance, occurring around the time of the LED onset (LED ON), is evident in Fig. 12. At fixation onset (FIX epoch), the recognition rate reached its peak and remained constant in the subsequent delay interval (DELAY) and in the reaching execution (REACH). Interestingly, after the reaching, the gaze and the hand still remained on the target, whereas the decoding accuracy decreased. This suggests that the decoding performance is strictly linked to the preparation and execution of reaching, instead of being linked to the gaze fixation of the target, as documented by decoding results shown from a control experiment in Fig. S2. In the task used in the main text (see Fig. 10 C-D), gaze position and reach goal were coincident. Rather than related to reach goals, one could argue that the predictions of our classifier were related to gaze position-and/or reach preparation-related activity (Hadjidimitrakis et al., 2011, 2012; Breveglieri et al., 2012, 2014). To uncouple the decoding of gaze and reach goals, 67 neurons out of 83 of the original population were recorded while monkey M2 performed a delayed reaching task towards the same nine targets of the original task with the gaze fixed on the central position (Constant-gaze task). A yellow flash (Cue), in the early phase of the delay, instructed the monkey about which target should be reached for. In the Constant-gaze task the increase of tuned cells occurs at cue onset, i.e. when the monkey receives instruction about the location of the target to be subsequently reached for. On the contrary, in the same neurons (N=67) tested in the Fixation-to-reach task, the increase of tuned cells occurred at the fixation onset, because in this task the fixation LED per se instructed the monkey about the reach

goal location. The same trend was also observed in the decoding performance: the accuracy was very low during fixation before the cue and increased immediately after the cue was given. This rules out the possibility that gaze fixation *per se* is responsible for the high decoding performance achieved in the Fixation-to-reach task. The accuracy shown in the confusion matrices from the Constant-gaze task is not significantly different from the results of the same population of cells when tested for the Fixation-to-reach task (results for the Fixation-to-reach task for the 67 cells tested for both tasks: 90% (SD 4.1) for FIX epoch, 98% (SD 2.2) for DELAY epoch and 88% (SD 4.9) for REACH epoch, t-test  $p > 0.05$ ). Neuron dropping and sliding window analyses (fig. S2D-E) support the evidence that, as soon as the visual cue was provided, the decoding performance reached optimal values for both Constant-gaze and Fixation-to-reach tasks. The data of the control experiment highlight that gaze information is not necessary to obtain high decoding accuracy from area V6A.

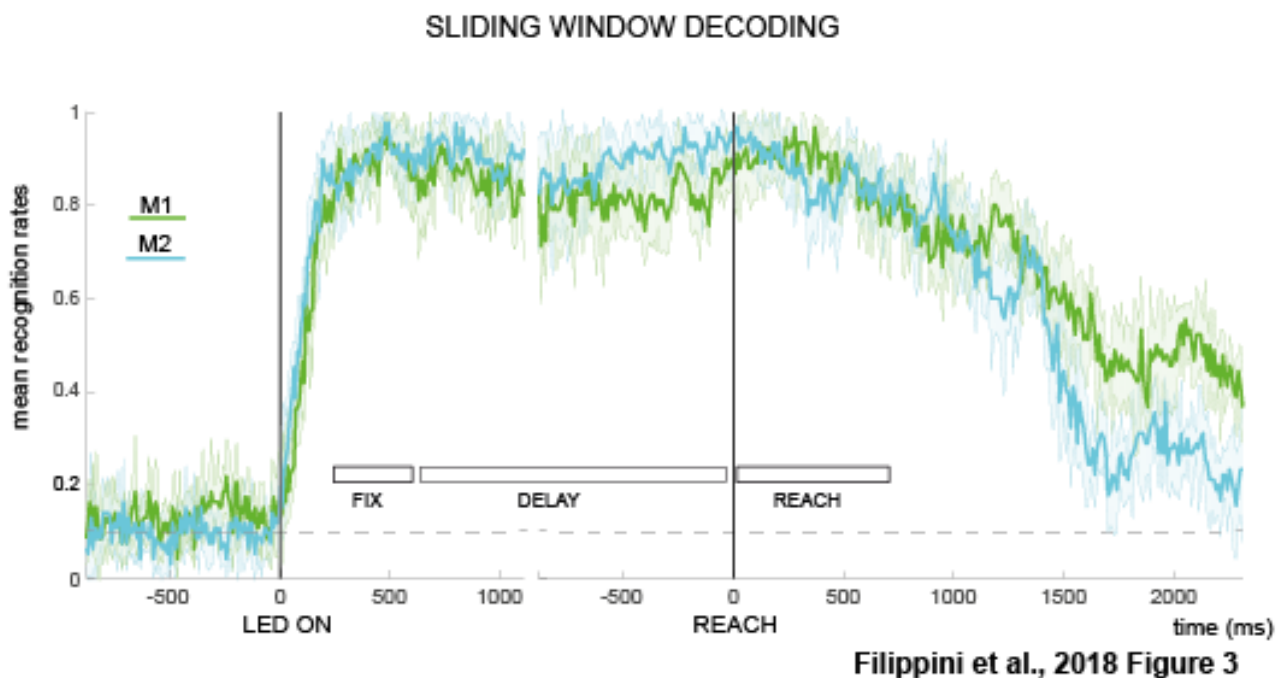


**Figure 12.** Sliding window decoding analysis. Time course of the decoding accuracy (recognition rates) based on the firing rates extracted during the period starting 1 s before the target illumination (LED ON), till 2 s after the movement onset (REACH). Due to the variable duration of the delay interval (1.3–2.1s), double alignment result plots are shown. Firing rates were calculated for a 300 ms sliding window, moving forward with a 10 ms step. Each dot on the graph was plotted at the beginning of the 300 ms window. The mean lines were calculated as the arithmetic mean between recognition rates of individual target positions. For each position, variability bands are shown, representing standard deviations based on a five-fold cross-validation.

**4.3.4. Generalization analysis.** To evaluate whether the neural code used during the early fixation period was retained or changed during the subsequent planning interval before the reach movement, we performed a generalization analysis by training decoders either in FIX or in REACH epochs, then we applied both codes on these epochs and portions of the DELAY epoch. Figure 13 shows the results of this analysis for the two monkeys. The code learned during the early fixation period (FIX, blue line) was gradually lost in the DELAY intervals; the accuracy then dropped during movement execution (~20%). This suggests that the neural code used during the earliest fixation phase became progressively weaker as soon as the animal began to prepare the movement. The time course of the accuracy obtained by training the algorithm with the movement neural activity (REACH, red line in Fig. 13), and testing the algorithm with the DELAY activity demonstrated that the neural code used during the action execution was partially preserved also during the last part of the planning period, but not in the earlier planning phases and initial fixation. In summary, by looking at the activity during early fixation, it was not possible to predict the spatial position during reach execution and vice versa. When the accuracy of the classifier trained in the different fractions of the DELAY was analyzed (grey lines in Fig. 13C, D), progressive code transformations were present. Both monkeys depicted a smooth transition between an earlier code, possibly related to the gaze location information, and a later code correlated with the movement preparation.

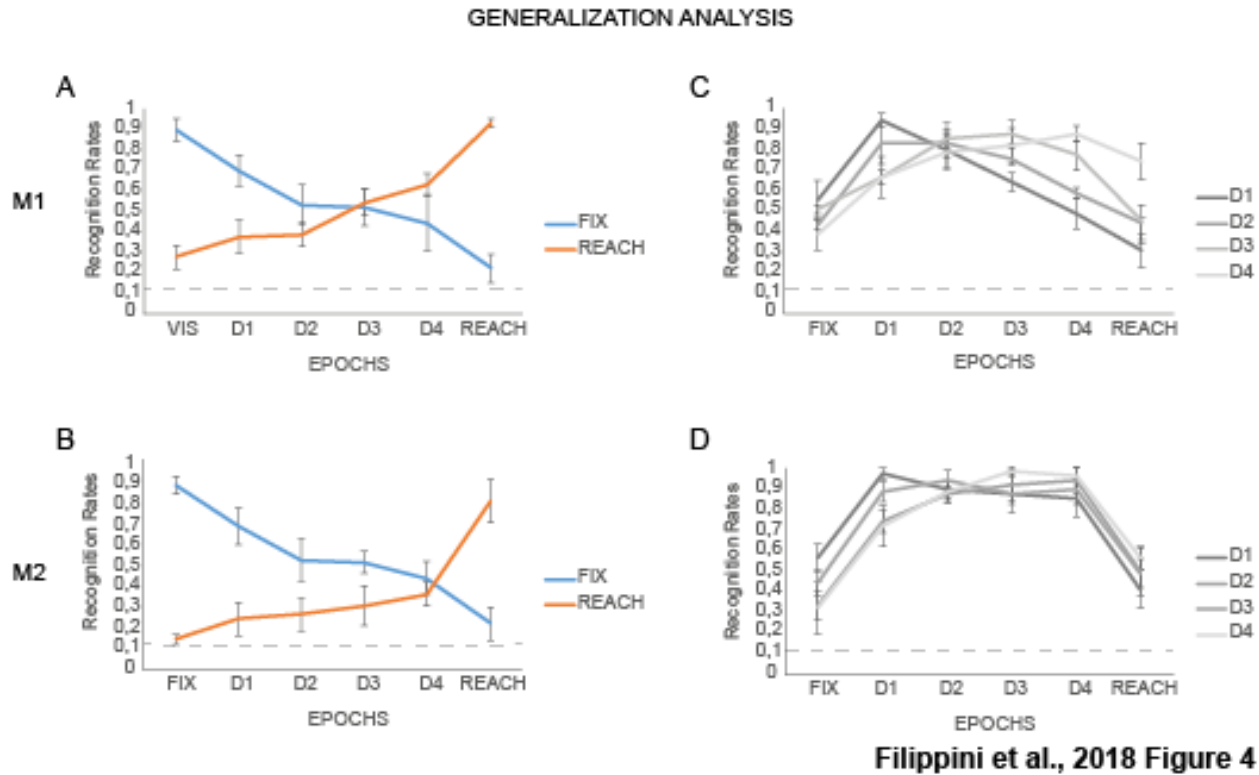


**Figure 13.** Generalization analysis. Generalization of codes derived from different epochs: the decoder was trained with the mean firing rates during one epoch and then tested to decode the other epochs. The trend of mean recognition rates together with the SD bars through different epochs are plotted as colored lines. Results are shown for the two monkeys M1 (A, C) and M2 (B, D). The DELAY epoch was split in portions due to variable time duration between the trials: D1, 0–25% of the delay epoch; D2, 25–50%; D3, 50–75%; D4, 75–100%. (A, B) Blue line shows the decoder trained on FIX, red line shows the decoder trained on REACH. (C, D) the decoder was trained on fractions (different grey scales) of the DELAY epoch.

#### 4.4. Discussion

In this study, we demonstrated that neural signals from area V6A can be successfully used for the offline decoding of reach goals located at different depths and directions, in conditions similar to everyday life, where reaching movements are performed not only on a single plane, but also in 3D. In most cases, just a few neurons (~20) were sufficient to achieve a correct prediction. The accuracy of decoding was optimal from early target fixation to the end of reaching.

We used a task configuration where the monkeys fixated the goal of reaching movement, which is the most physiological condition (Neggers and Bekkering, 2001; Hayhoe et al., 2003). However, this setup cannot distinguish whether decoding uses gaze signals or arm movement-related activity. To exclude gaze-related activity from decoded signals, we performed decoding in another

experiment in which the monkey performed a task where gaze and reaching targets were not coincident (figure S2). In this case too, decoding performance was very high. This result is in line with the strong spatial tuning in V6A reach-related activity when gaze is dissociated from the reach target position (Bosco et al., 2016). However, in our study, we did not test decoding in a free gaze condition, where gaze was truly independent. Thus, we cannot exclude the possibility that eye movements could potentially disturb the decoding from V6A. However, the very similar results obtained between tasks (fig. 12 and fig. S2E) suggest that free gaze should not interfere with decoding reliability from V6A. Nevertheless, these results suggest V6A as a source for brain computer interfaces (BCIs), not only when the patient can move his/her eyes to the reaching target, but also in the absence of ocular motility.

#### 4.4.1. Decoding reach goals from parietal cortex

Several monkey studies performed decoding of reach goals (Shenoy et al., 2003; Musallam et al., 2004; Scherberger et al., 2005) and trajectories (Mulliken et al., 2008a) in 2D space from activity in PPC (specifically, from the parietal reach region, PRR). Here, we decoded reach goal from another part of PPC, while also considering the depth dimension.

In V6A, target location was decoded from neural responses occurring not only during reaching execution, but also well before the movement onset. This is similar to the neighboring PRR area, where neural signals during reach planning were used to online decode up to 6 reach goals on a screen and to guide a cursor (Musallam et al., 2004). Accuracy obtained in PRR was lower than in V6A (from 25% to 60% in PRR, (Musallam et al., 2004) vs about 90-100% in V6A, present results). However, differences in the experimental design may account for these discrepancies.

Here, the trajectory of the reaching movement could not be extracted, since only information on the reach goal location was available. Nevertheless, it was demonstrated that goal specificity is advantageous for ballistic operations (Musallam et al., 2004) and that by incorporating information about the reach goal (target position), the decoding accuracy of the trajectory estimation from PRR signals improved by 17% (goal-based Kalman filter, Mulliken et al. 2008). Alternatively, the optimal reconstruction of movement trajectories could be performed by computer vision (Andersen et al., 2014; Katyal et al., 2014).

Looking at current state-of-the-art neural prosthesis technology, in order to increase prosthesis reliability we need to increment the number of neurons sampled. This involves overcoming several technical limitations and using more invasive implants. Intuitively, a mixed neural signals-computer vision driven BCI looks more feasible. From the PPC region we can retrieve intention of movements, and this information could aid computer vision systems to be 'mind controlled' or classic motor BCIs (i.e. BCIs driven by motor cortex) to reconstruct the movement smoothly, knowing movement goals in advance. Exploiting higher-order, multidimensional information for decoding purposes could allow the development of more natural and user-friendly brain-machine interfaces to achieve fully integrated prehensile actions.

#### 4.4.2. Decoding of depth information for reaching

An important novelty of our study is the decoding of reaching goals from signals in PPC, also taking into account the depth dimension. Several studies demonstrated the feasibility of retrieving instantaneous movement attributes, such as position, velocity and acceleration useful to drive artificial limbs in 3D space (Brandman et al., 2017). This has been achieved using activity from motor and premotor regions in monkeys (Taylor et al., 2002; Carmena et al., 2003; Jarosiewicz et al., 2008; Velliste et al., 2008) and in humans (Hochberg et al., 2012; Collinger et al., 2013). In monkey PPC (areas PRR and 5d), continuous trajectory reconstruction of cursor movements in a 3D virtual space was demonstrated by Hauschild and coworkers (Hauschild et al., 2012). In that study, a good decoding performance ( $R^2 \sim 40\%$ ) was obtained using ensembles of about sixty neurons.

BCI applications that restore basic interaction with objects in tetraplegic patients have recently been reported (Hochberg et al., 2012; Collinger et al., 2013; Aflalo et al., 2015). These studies demonstrated the feasibility of BCIs in humans, but there is much work still to be done. When the depth information was added, movements became reasonably slower and clumsier (Collinger et al., 2013). Thus, our results showing reliable decoding not only in 2D, but also in depth, are of particular importance.

#### 4.4.3. Decoding entire prehension from V6A

V6A has recently been suggested as a site of convergence of arm signals for reaching and grip signals for grasping to direct our hands towards efficient prehensile actions (Gardner, 2017; Galletti and Fattori, 2018). In humans, fMRI signals from a region that is a likely homologue of monkey V6A (Pitzalis et al., 2013) were used to successfully predict the direction of an upcoming reach, but not of a saccade (Gallivan et al., 2011b). In a recent study, Nelissen et al (Nelissen et al., 2018) decoded grasping-related information from fMRI signals in monkey area V6A. This finding complements the decoding of the type of grasp (Filippini et al., 2017) and reach goals (present results) and suggests that V6A could be a useful site for the neuroprosthetic control of the entire prehension action.

#### 4.4.4. Potential applications and future directions

Despite the tremendous advances in neural prosthetics based on signals from the motor cortex, the future of BCIs relies on the acquisition of neural signals that also reflect the cognitive state of the patient, i.e. intentions and movement goals (Andersen et al., 2014). These cognitive prostheses may be implemented by decoding neural signals from parietal regions, like V6A, so as to have signals related to movement intention and execution from the same area. V6A incorporates signals typical of parietal regions (intentions of movement), but also signals coding for some useful details of the movement, such as depth and direction of reaching, and even grip type (Filippini et al., 2017). This intelligent prosthetics is one potential application of the results presented here.

Another potential and promising application of decoding arm actions from V6A is in the emerging field of soft robotics, a technology born mimicking natural beings, to replace classical rigid-bodied robots with limbs that are more comfortable and easy-to-handle (Rus and Tolley, 2015). Although soft robotics is becoming more and more popular, the potential of soft machines in the clinical field is still greatly under-exploited, mainly because of limited functionality and versatility caused by the lack of intelligent, natural control systems. Indeed, so far soft robots have been relying on classic control approaches that reduce the advantages of “soft” robotics in terms of flexible interaction with a variable environment. A direction for the very near future is to design more intelligent soft robots taking advantage of bio-inspired controllers that will be developed thanks to

advances in artificial intelligence and inspired by the neurophysiology of our bodies (Fani et al., 2016; Santello et al., 2016). For a new generation of user friendly prostheses like these biomorphic robots, natural signals with multiple neural information like those from V6A might be exploited for a more dexterous control of artificial limbs.

## 4.5. Experimental procedures

**4.5.1. Experimental procedure.** The study was performed in accordance with the guidelines of EU Directives (86/609/EEC; 2010/63/EU) and Italian national laws (D.L. 116-92, D.L. 26-2014) on the protection of animals used for scientific purposes. Protocols were approved by the Animal-Welfare Body of the University of Bologna. During training and recording sessions, particular attention was paid to any behavioral and clinical sign of pain or distress. For surgical and electrophysiological procedures, see Hadjidimitrakis et al., (2014). Two male monkeys (M1 and M2, aged 5 and 8 years) were involved in the study.

**4.5.2. Equipment and Behavioral Task.** Electrophysiological data were collected while monkeys were performing a Fixation-to-reach task with the contralateral limb (with respect to the recording hemisphere), with the head restrained, in darkness, while maintaining steady fixation of the target. Reaches were performed to one of nine light-emitting diodes (LEDs; 6 mm in diameter, Fig. 10C). The LEDs were mounted on a panel located in front of the animal, at different distances and directions with respect to the eyes, but always at eye level.

Given that the interocular distance for both animals was 30 mm, the nearest targets were located at 10 cm from the eyes, whereas the LEDs placed at intermediate and far positions were at a distance of 15 and 25 cm, respectively. Because targets were aligned at eye level, they could potentially obscure each other. We solved the problem by masking the nearest LEDs to be visibly thinner than second line LEDs and the latter thinner than the farthest line. Thus, the monkeys were able to easily discriminate them.

In the task, the monkeys pressed a button located close to their chest (HB, Fig. 10C), fixated one of the targets for a variable period (FIX, Fig. 10D left), prepared the movement (DELAY; Fig. 10D center) and started the reaching movement (REACH, Fig. 10D right) towards the foveated target.

**4.5.3. Data analysis.** The analyses were performed with customized scripts in Matlab (Mathworks; RRID:SCR\_001622) and Python (using open-source machine learning toolkit scikit-learn, <http://scikit-learn.org>; RRID:SCR\_002577). The neural activity was analyzed by quantifying the discharge in each trial in the following three different epochs (Fig. 10D).

Fixation-to-reach task:

- 1) the early fixation epoch (FIX), from 50 ms after the end of the saccade performed to gaze at the LED till 450 ms after it;
- 2) the preparation epoch (DELAY), from 450 ms after the end of the saccade to the arm movement onset. Given the task structure and the variable reaction time of the monkeys, this epoch had a variable duration (from about 1.3s up to 2.1s);
- 3) the reach epoch (REACH), from the arm movement onset (M) till the end of it, signaled by the pressing of the LED target.

All the analyses and modeling were done off-line. Among the original set of recorded neurons, we considered only cells with at least 10 trials for each of the nine targets. All recorded neurons, either modulated in the reaching task or not (see Supplemental Experimental Procedures), were used in the decoding analysis.

**4.5.4. Neural decoding.** For each neuron of the population (181 neurons for M1, 83 for M2, respectively), we computed the mean firing rate (mFR; number of spikes per time units) over a selected timespan using a trial-by-trial approach. The decoder outputs were the 9 targets. Fivefold cross-validation was performed by using 72 samples (eight for each condition) for training and 18 (two for each condition) for testing for each neuron, to ensure that the classifier was trained and tested on different data. Recognition rates and SD were calculated as means over the five folds' iterations. Not normalized data were used for the decoding procedure.

We used a naive Bayesian classifier as decoding algorithm. Naive Bayes methods are a set of supervised learning algorithms based on applying Bayes' theorem with the "naive" assumption of independence between every pair of features. This technique has been shown to achieve performance closer to optimal compared with other classifiers such as Support Vector Machine (SVM) when analyzing neural data (Carpaneto et al., 2011; Schaffelhofer et al., 2015). In our Python custom scripts, we implemented the module of naïve Bayes classifiers proposed by *scikit-learn* libraries (the statistical formulation can be found at <http://scikit-learn.org>).

[learn.org/stable/modules/naive\\_bayes.html](https://learn.org/stable/modules/naive_bayes.html), (Zhang, 2004)). Under the assumption of Poisson distribution of features, we reinforced the model as suggested at the following site: <http://github.com/scikit-learn/scikit-learn/pull/3708/files> (Ma et al., 2006). We performed three types of analysis, computing the following feature vectors over different epochs and timespans: whole epoch, sliding window, and generalization analysis. The same kinds of analyses have been performed in area V6A from different sets of neurons recorded in a grasping task (Filippini et al., 2017).

## 4.6. Supplemental Experimental Procedures.

Two male macaque monkeys (*Macaca fascicularis*, monkeys M1 and M2) with a weight ranging between 4 and 4.4 kg were involved in this study. A head-restraint system and a recording chamber were surgically implanted in asepsis and under general anesthesia (sodium thiopental, 8mg/kg/h, i.v.) following the procedures reported by Galletti et al., (1995) and Hadjidimitrakis et al., (2014). Adequate measures were taken to minimize pain or discomfort. A full program of postoperative analgesia (ketorolac trometazyn, 1mg/kg, i.m., immediately after surgery, and 1.6 mg/kg, i.m., on the following days) and antibiotic care [Ritardomicina (benzathine benzylpenicillin plus dihydrostreptomycin plus streptomycin), 1–1.5 ml/10 kg every 5–6 d] followed the surgery.

We performed extracellular recordings from the posterior parietal area V6A (Galletti et al., 1999b) using single-microelectrode penetrations with home-made glass-coated metal microelectrodes (tip impedance of 0.8–2 MOhm at 1 kHz) and multiple electrode penetrations using a five-channel multielectrode recording mini matrix (Thomas Recording). The electrode signals were amplified (at a gain of 10,000) and filtered (band pass between 0.5 and 5 kHz). Action potentials in each channel were isolated with a dual time–amplitude window discriminator (DDIS-1, Bak Electronics) or with a waveform discriminator (Multi Spike Detector, Alpha Omega Engineering). Spikes were sampled at 100 kHz and eye movements were simultaneously recorded using an infrared oculometer (Dr Bouis, Germany, for M1, and ISCAN for M2) and sampled at 100 Hz. All neurons were assigned to area V6A following the criteria defined by Luppino et al. (Luppino et al., 2005) and described in detail by Gamberini et al. (Gamberini et al., 2011).

**4.6.1. Behavioral task.** The time sequence of the task was the same used in Hadjidimitrakis et al., (2014). A trial began when the monkey pressed a home button (HB; 2.5 cm in diameter) located

next to its trunk (Fig. 10C). After 1 s, one of the nine LEDs was switched on to green. The monkey had to fixate the LED while keeping the HB button pressed. The monkey then had to wait 1.5–2.5s for a change in the color of the same LED (from green to red) without performing any eye or arm movement. The color change was the go signal for the animal to release the HB and to start an arm movement toward the target. The monkey then reached the target and held its hand on the target for 0.8–1.2s. The switching off of the target cued the monkey to release it and to return to the HB, which ended the trial and allowed the monkey to receive its reward. The presentation of stimuli and the animal's performance were monitored using custom software written in LabVIEW (National Instruments), as described previously (Kutz et al., 2005). Eye position signals were sampled with two cameras (1 for each eye) and were controlled by an electronic window ( $4^\circ \times 4^\circ$ ) centered on the fixation target. If the monkey fixated outside this window, the trial was aborted. The task was performed in darkness, in blocks of 90 randomized trials, 10 for each target position. The luminance of the LEDs was adjusted to compensate for difference in retinal size between LEDs located at different distances. The background light was switched on between blocks to avoid dark adaptation.

At the beginning of each recording session, the monkey was required to perform a calibration task gazing at targets on a frontal panel placed at a distance of 15 cm from the eyes. For each eye, signals to be used for calibration were extracted during fixation of five LEDs arranged in the shape of a cross, one centrally aligned with the eye's straight-ahead position and four peripherally placed at an angle of  $\pm 15^\circ$  (distance 4 cm) in both the horizontal and vertical directions. From the two individual calibrated eye position signals, we derived the mean of the two eyes (conjugate or version signal) and the difference between the two eyes (disconjugate or vergence signal) using the following equations:  $\text{version} = (R + L)/2$  and  $\text{vergence} = R - L$ , where R and L are the gaze direction of the right and left eye, respectively, expressed in degrees of visual angle from the straight-ahead direction. The version and vergence values were also used by the LabVIEW software to control the gaze position.

In the Fixation-to-reach task, the fixation target was always coincident with the reaching target. Given that the target was foveated in all epochs of interest, its depth and direction in space were equal to the vergence and version angles of the eyes, respectively.

**4.6.2. Control task.** In one case (M2), we performed an additional task. The monkey performed a Constant-gaze reaching task (fig. S2), where the reaching movement was executed maintaining

gaze fixation on the central, straight-ahead position. Keeping the fixation point constant allowed constant vergence and version eye signals and precluded cell responses resulting from the eye vergence and version signals, known to affect V6A neural discharges (Breveglieri et al., 2012, 2015). The monkey was instructed to fixate the central position during the task execution. After 700 ms from the onset of the fixation LED, a yellow LED (CUE) was illuminated for 150 ms in the location where the monkey then had to subsequently reach. After the switching off of the CUE, the monkey had to wait for the change in color of the fixation LED to perform the reaching movement, in the same way as the Fixation-to-reach task. In the Constant-gaze task, the neural activity was analyzed by quantifying the discharge in each trial in the following different epochs (fig. S2):

- 1) FIX\_CG epoch: from 50 ms after the end of the saccade performed to gaze at the LED till 450 ms after it;
- 2) CUE epoch: from cue onset till 400ms after it;
- 3) DELAY\_CG epoch: from 400ms after the cue onset till the movement onset;
- 4) the reach epoch (REACH\_CG), from the arm movement onset till the end of it, signaled by the pressing of the LED target.

**4.6.3. Neuron dropping.** The number of units required to give a sufficient amount of information to efficiently decode the target position in space is not a trivial amount of information for the development of BMI applications. This is why we performed the neuron dropping analysis that measures the decoding accuracy as a function of neurons used for decoding (Figs. 11B and S2D). This analysis was performed on all the epochs of interests. This algorithm started by training the decoder with a randomly selected neuron. The number of cells included for decoding was then increased in steps of 1 until all available neurons were included. At each step, the random selection of cells used for decoding was repeated 100 times.

**4.6.4. Sliding window decoding.** For the sliding window analysis, mFRs were computed over a window of 300 ms, which progressively slid over the reference period with a moving step of 10 ms. As in the previous case, training and testing sets were computed over the same time interval. This approach (Figs. 12 and S2E) was used to see how the recognition rate changed dynamically over time.

4.6.5. **Generalization analysis.** We employed a generalization analysis, also used in one of our recent reports (Filippini et al., 2017). For the generalization analysis (Fig. 13), mFRs were computed over different intervals for training and testing sets: the system was trained over the whole FIX and REACH epochs and over four parts of the DELAY epoch; after training the system for an epoch, it was tested over all the epochs. This was done to verify whether the same code is used from early target fixation to movement execution, or to discover how the code changes during the epoch, before the movement, and during movement execution. As the DELAY epoch varied in duration from trial to trial (~1.3-2.1s; with a mean of 1.72s, SD 0.29), we performed the generalization analysis on 25% fractions of DELAY rather than on fixed size intervals. In all experiments, classification performance was assessed by the rate of correct recognitions, and confusion matrices. These representations helped to reveal the most common error patterns of the classifier.

4.6.6. **Population response.** Population response of all the recorded cells was calculated as averaged spike density function (SDF; Fig. S10A). An SDF was calculated (Gaussian kernel, half-width 40 ms) for each neuron included in the analysis, and averaged across all the trials for each tested target. The neuron peak discharge found over all targets during the REACH epoch was used to normalize all SDFs for that neuron. The normalized SDFs were then averaged to obtain population responses (Marzocchi et al., 2008). Each condition was ranked based on REACH discharge and aligned twice in each plot, one on LED onset, and the other on movement onset. Double alignment was required because of the variable duration of the DELAY epoch.

We performed a sliding one-way ANOVA (factor: LED position, 9 levels,  $p < 0.05$ , figs. S1B and S2B) to investigate the tuning of the population for the spatial position across the time course of the task. Mean firing rates of each neuron were calculated for an arbitrary chosen 300 ms window which slid forward with a 10 ms step. The incidence of ANOVA significant cells is plotted in Figures S1B and S2B.

4.6.7. **Comparison between the results of Fixation-to-reach task and Constant-gaze task.** We statistically compared the results of the Fixation-to-reach task and Constant-gaze task with a permutation test (10,000 iterations) comparing the sum of squared errors of the actual and randomly permuted data (see (Marzocchi et al., 2008)).

## 4.7. Supplemental Figures

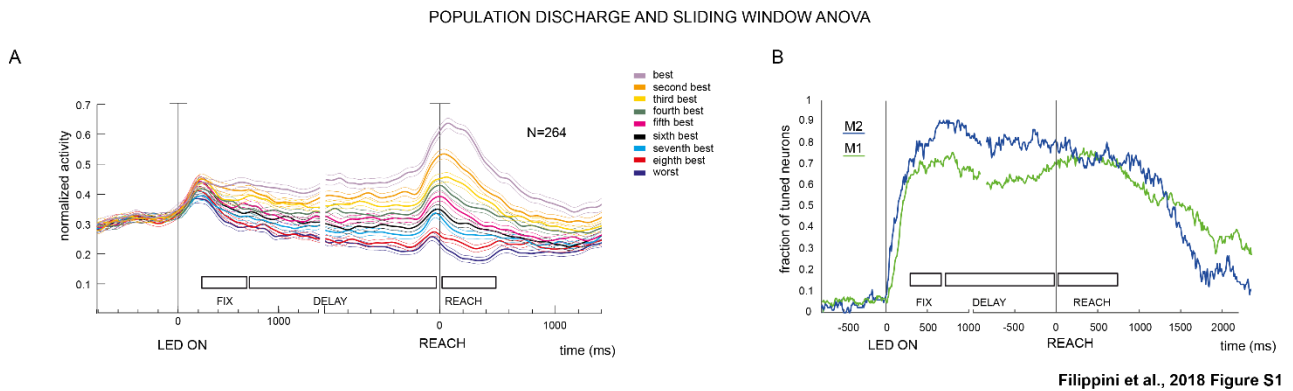


**Figure S1. Population discharge and tuned cells during the reaching task, Related to Figure 3.** A) Activity of V6A neurons used for the decoding procedure expressed as averaged normalized SDFs (thick lines) with variability bands (Standard error of the mean, thin lines), constructed by ranking and normalizing the response of each neuron for each individual target according to the intensity of the response elicited in the REACH epoch in descending order (from violet to dark blue). Data have been aligned twice, one (left) on LED onset (LED ON), one (right) on movement onset (REACH). The SDFs of each alignment were calculated on the same population of cells. Each cell of the population was taken into account nine times, once for each target position. Scale on abscissa, 200 ms/division (tick); vertical scale, normalized firing rate frequency. B) Tuned cells during the Fixation-to-reach task. Individual curves describe the fraction of tuned units versus time (sliding window ANOVA, factor: LED position, 9 levels,  $p < 0.05$ , 300 ms window sliding with a 10 ms step) separately for M1 (green line) and M2 (blue line). Each dot on the graph was plotted at the beginning of the 300 ms window used for the sliding ANOVA. Other conventions as in Fig. 3. The plot shows changes in the fraction of tuned cells as the task progresses. Many V6A neurons responded significantly to target fixation. The peak was reached around 500 ms after the LED onset (that drove the fixation onset), then the fraction of tuned cells remained quite stable in the DELAY and REACH epochs. Finally, the number of tuned cells began to decrease at the end of the reaching movement, after the target touching, i.e. at the end of the REACH epoch. Overall, ~65% of cells were modulated by the spatial position of the target in monkey 1 (M1) and ~80% in the second monkey (M2), with similar trends over time.

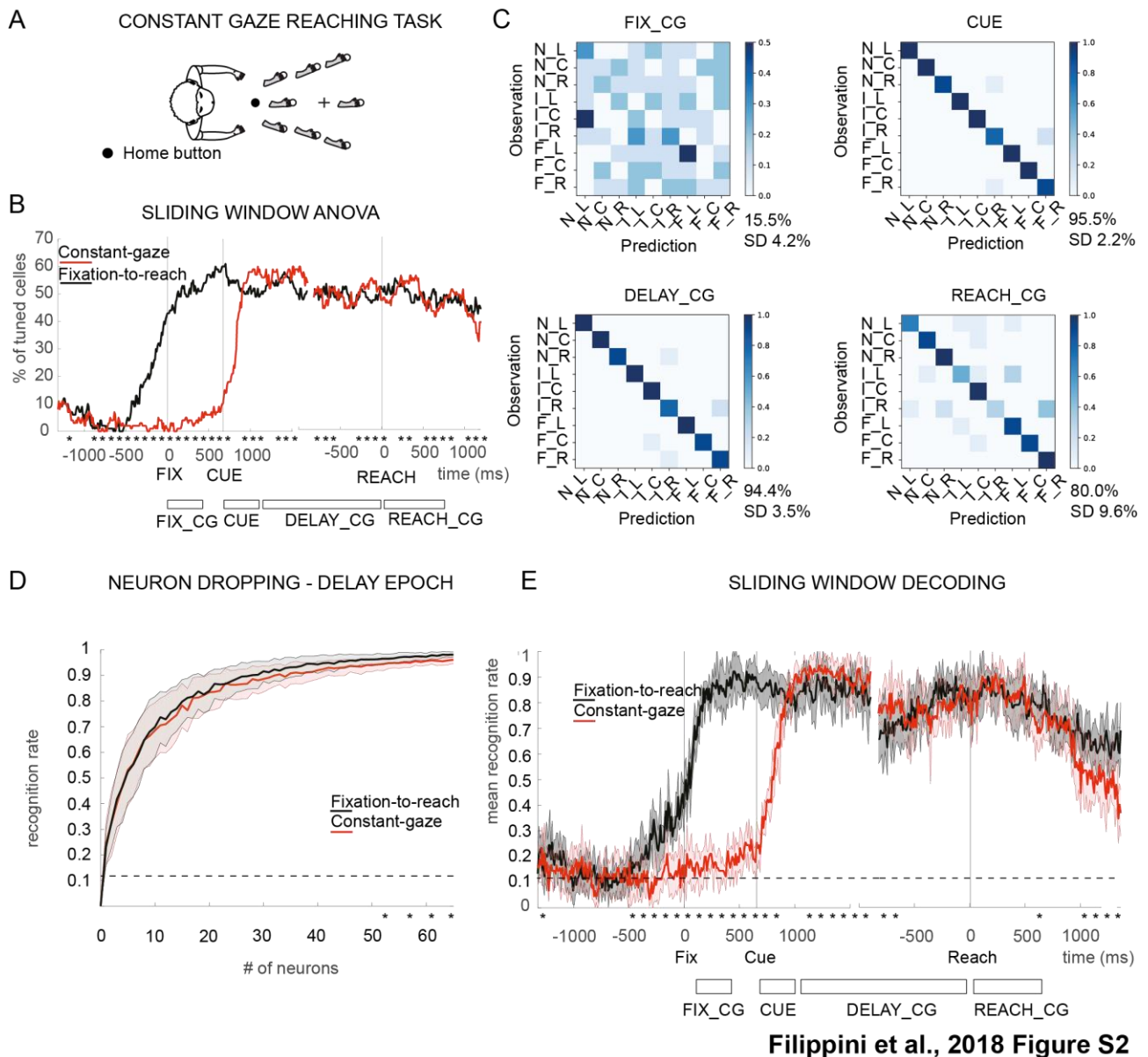


**Figure S2. Results of the control experiment run for M2, Related to Figures 2-3.** A) Constant-gaze task setup. The monkey had to keep the fixation on a central position (cross) while performing instructed-reaching toward goals placed in the positions indicated by the little hands, located at 3 depths and 3 directions around the central gaze position (circles). B) Sliding ANOVA describes the percentage of tuned neurons ( $p < 0.05$ ) as a function of time. Asterisks under the x-axis indicate statistically significant differences between lines (permutation test, 1000 iteration,  $p < 0.05$ ). Alignments from left to right: fixation onset, cue onset, reach onset. C) Confusion matrices calculated in the Constant-gaze reaching task for epoch FIX (FIX\_CG), CUE, DELAY (DELAY\_CG) and REACH (REACH\_CG). The matrices summarize the results of cross-validation iterations plotted as real class (Observation) against predicted class (Prediction). Position of the reach goals: N\_L=Near left; N\_C= Near central; N\_R= Near right; I\_L= Intermediate left; I\_C= Intermediate central; I\_R= Intermediate right; F\_L= Far left; F\_C= Far central; F\_R= Far right. D) Comparison of neuron dropping results between Fixation-to-reach (black line) and Constant-gaze task (red line). Standard Deviation is reported as colored shadows. Asterisks under the x-axis: statistically significant differences between lines (t-test,  $p < 0.05$ ). Below 50 neurons the 2 curves do not show any difference. E) Sliding window analysis for Constant-gaze task (red line) superimposed to Fixation-to-reach task results (black line). Cue onset is also shown (Cue). Asterisks under the x-axis: statistically significant differences between lines (t-test,  $p < 0.05$ ). Other conventions as in figs S2, 3. The neural coding during the Fixation-to-reach task and the Constant-gaze reaching task was not consistent. This is in agreement with the strong influence of

the reference frames in V6A cells (Bosco et al., 2015, 2016). In these studies, we documented that the discharge of many V6A cells changed according to the relative positions of gaze and arm. We also found that the decoder trained on the Fixation-to-reach task could not predict the correct position using data from the Constant-gaze task (data not shown). This suggests that a different code was used through the two different tasks.

## 5. General discussion

The posterior parietal cortex participates in multiple cognitive processes including sensorimotor integration, spatial attention, decision making, working memory, motor planning (Whitlock, 2017). Signals from different areas of PPC have been used to decode potential reach plans, from parietal reach region (PRR), spatial positions of reaching goals and trajectories, from area 5d, hand postures for grasping, anterior intraparietal area (AIP), and saccades, from lateral intraparietal area (LIP) (see Andersen et al., 2014 for a review). Traditionally, reaching and grasping networks were separated into dorsomedial and dorsolateral visual stream, respectively (Kandel et al., 2013). Area V6A, located in the caudal PPC is one of the first nodes of the reaching network, but has been found to encode for both reach and grasp components of prehension (Fattori et al., 2005, 2009, 2010; Breveglieri et al., 2016, 2018). The aim of my project was to test whether reaching and grasping signals recorded from V6A can be decoded and so to demonstrate that a single area can potentially be used to guide prosthetic arms performing full prehension. For this purpose, we conducted two separate experiments where monkeys were trained to either perform a reaching or a grasping task.

In a first experiment monkeys had to grasp five objects; the five objects were chosen with different shapes to induce different grips from the most rudimentary to the most skilled. The spatial position of the objects was identical for all objects, a rotating panel presenting one object at time, so no spatial parameters were encountered. Before the actual movement, the monkey had to wait for a go signal. This was useful to study preparatory neural activity and, in the case of dark condition, where the object was illuminated only for 500ms and the movement was performed in the dark, it permitted to uncouple visual- from motor-related activity. Population activity ranked for preferred object (SDF, Fig. 6B) suggested that most of neurons modulated their activity according to the object observed or grasped by the monkey. This was a good hint on the possible application of machine learning techniques. Pooling together mean firing rates of the neural population (features vector), a ML algorithm can learn the activation patterns of neurons in a given condition. The trained model could be used to predict the correct object, given population firing rates. Doing so (Filippini et al., 2017), results showed that firing rates of 79 neurons recorded from V6A were predictive of the object observed or grasped, misclassifications were very

uncommon (see Fig. 7). Although limited to 5 types of grips, this was the first evidence that signals from dorsomedial visual stream may be used to control grasp aspects of a prosthetic hand.

In a second experiment monkey had to reach for 9 different targets arranged in the peripersonal space. The reaching task was once again a delayed task: the movement was preceded by a waiting interval where the animal fixated only the target, no movements were permitted. Firing rates from 264 neurons were used to train a classifier to predict the position reached by the monkey (Filippini et al., 2018). The decoder was very accurate in predicting the right position, even though the 9 targets were distributed over a limited 12x15cm spatial volume 10cm away from monkey. Targets were always foveated so a good question was whether the decoder was just predicting the eye position. Eye signals are present in V6A (Galletti et al., 1995; Breveglieri et al., 2012) but decoding results on a control task confirmed that this was not the case, predictions were still accurate though reaching goal and eye position were uncoupled (fig S2E). Several monkey studies decoded reaching goals (Shenoy et al., 2003; Musallam et al., 2004) and trajectories (Mulliken et al., 2008a; Torres et al., 2013) from PPC. In these studies, targets were displayed on a screen or showed on a 2D LEDs matrix, the depth dimension was always neglected. Area V6A encodes for directions and depth (Hadjidimitrakis et al., 2011, 2014a), accordingly the decoder accurately discriminated positions on different depth levels. Together, decoding of direction and depth allow the fine reconstruction of reaching in the 3D space.

## 5.1. PPC for decoding

One of the main advantages for using PPC as source for decoding and neuroprosthetic is that preparatory activity carries the information of intended goals. Indeed, we were able to decode reaching goals and type of grips well before the actual movement was performed. Having this information as soon as possible is desirable for neuro prosthetic applications (Andersen et al., 2010, 2014; Hadjidimitrakis et al., 2019). Signal acquisition, preprocessing, decoding and the actual movement of the prosthesis are steps that require time, the accumulated latency can make the use of the prosthesis unnatural. Besides neuro prosthetics, neural decoding is a powerful tool to gain new insight on dynamics of neural encoding. Generalization analysis showed that different codes alternate during task execution. In both grasping and reaching, a decoder trained with data from the first part of the task (object vision or early target fixation) could not be generalized for

the movement phase and vice versa. This supports the model of a sensorimotor transformation that occurs in PPC (Gail and Andersen, 2006). The simultaneous presence of sensory input and motor-related activity found in V6A suggested a model where V6A could contribute to online control of the movement. Working as comparator between the expected state of arm movement and the visual/somatosensory feedback evoked by the movement itself, V6A could compute the mismatch supporting the movement correction (Fig.14) (Bosco et al., 2010; Fattori et al., 2017).

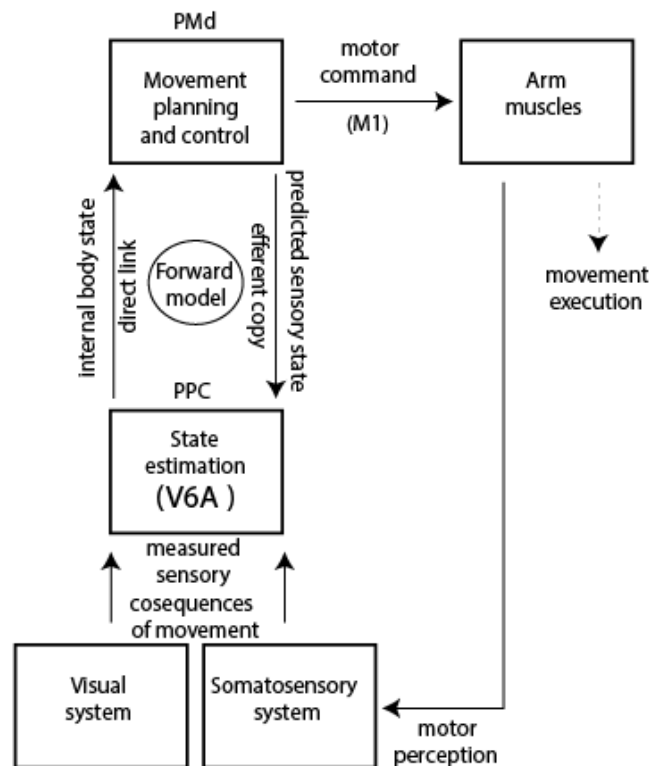


Figure 14. Neural circuitry involving area V6A in the neural control of movement. A flow chart of a possible circuit involving V6A in the control of reach-to-grasp movements. Sensory information may be sent by V6A to dorsal premotor cortex (PMd), to which it is directly connected. V6A may be involved in the comparison of the anticipated motor plan with the current sensory feedback produced by moving hand and by visual background. Figure modified from Fattori et al., 2017.

A possible problem is the delay between movements and the resulting sensory feedback: visual signals take approximately 90ms (Raiguel et al., 1999) and somatosensory signals take 20 to 40ms (Allison et al., 1991) to reach the PPC. Inevitably this latency is increased due to sensorimotor integration (Flanders and Cordo, 1989; Wolpert and Miall, 1996). Our brain could predict the sensory consequences of a movement integrating an efferent copy of motor control coming from

premotor areas with the delayed sensory input. This forward model could compensate such latency and has been proposed to be integrated in PPC.

Mulliken and colleagues found that PRR neurons encoded for movement goal but also for dynamic heading angle toward the target, with a zero lag timing (Mulliken et al., 2008b). Consistent with a forward model, this was too late to be an output motor command and too early to come from a sensory input. Forward estimate has interesting implications for neuro prosthetic applications. A goal-based Kalman filter which combined forward estimate for trajectory and reaching goal information was superior to other decoders to move a cursor in a brain controlled task (Mulliken et al., 2008a). Considering that those data derived from a reaching area (the Parietal Reach Region), we can speculate that V6A could additionally provide information about grip type and other hand kinematics to be added to PRR performance.

## 5.2. Full prehension

Results here presented point toward a decoding of both reach and grasp components of prehension from a single area, V6A. A single site encoding for all the aspects of reach-to-grasp movement is advantageous for neural prosthetics. A single implant could potentially be sufficient to finely control a prosthesis to reproduce naturalistic movement. Furthermore, this implant could allow to achieve the control of both reaching and grasping. To my knowledge only another work tried to decode both reaching and grasping from PPC. Area AIP has been extensively studied by different authors and evidence relates this area with hand shaping for grasping (Taira et al., 1990; Sakata et al., 1995, 1997; Murata et al., 2000). To be noticed that area AIP is one of the critical nodes of dorsolateral visual stream, the traditional grasping network. Lehmann and Scherberger found that neurons in AIP represent grip type together with spatial signals, including gaze and retinotopic and spatial target positions (Lehmann and Scherberger, 2013). Approximately half of all neurons recorded contained spatial information, whereas grip type was encoded only by 30%. Decoding was very accurate, recognition rates were over 80% for combinations of different grip types and spatial reach positions. Chemical inactivation of AIP (Gallese et al., 1994) resulted in deficits in hand preshaping and grasping without impairment of reaching. This suggests that signals related to target position in AIP are not necessary for reaching. Instead these signals might assist the selection or generation of appropriate grasp movements (Lehmann and Scherberger

2013). Lesion of V6A resulted in deficit in reaching and also in grasping (Battaglini et al., 2002). Recently a tetraplegic human volunteer has been implanted with 2 Utah arrays in human putative AIP and Brodmann's Area 5. The two sites were pre-selected thanks to functional MRI scanning as areas particularly active during a grasping (AIP) and reaching (BA5) tasks (Fig. 10B). The patient was able to point different targets on a computer screen using a robotic arm under his volitional control (Aflalo et al., 2015). Moreover, up to 5 hand postures were decoded from the same neural signals (Klaes et al., 2015). Because of low yield of single unit from BA5 array, neurons from AIP and BA5 were pooled together to increase the decoder robustness. Unfortunately, performance of decoding for separate arrays was not available, yet this first attempt to decode both reach and grasp actions from PPC was promising. The alternative to solve the problem of recording from separate reaching (BA5) and grasping (AIP) areas could be recording from area V6A. Indeed, present results suggest that both components of prehension act can be reliably decoded from this area. Critical for BCI technology is implant invasiveness: electrodes inevitably damage the brain tissue, foreign materials trigger immune reaction, reducing the number of electrodes needed to guide prosthetics is always desirable. Thus recording from a single area all the information necessary to move a prosthesis is advantageous for clinical applications.

### 5.3. Limitations and Future directions

The joint results of reaching and grasping decoding demonstrated that simple classifiers can be used as neuro decoder to reconstruct reaching goals and type of grips. Although the classifiers are ideal in their simplicity for feasibility studies, they show their limitations in real applications. Indeed, especially for reaching problem, the space is a continuous physical quantity, reducing it to discrete quantity could be an excessive simplification. Decreasing the size of discretized spatial spots and increasing their number can be a fair trade off to model continuous space into easier to handle discrete space. Using this stratagem Bayesian decoder are still attractive and widely applied in research (some examples, Gao et al., 2002.; Shenoy et al., 2003; Scherberger et al., 2005; Bokil et al., 2006). Bayesian decoder are robust to intrinsic noise of neurons spiking activity. Interestingly they show parallels with brain function: modeling studies suggested that cortical areas may use Bayesian inference for decision making (Beck et al., 2008). The current state of art for continuous decoding are Kalman filters and modern derivatives. Again this class of decoder shows parallels with brain function. Kalman filter mimic the forward model and sensory feedback

with additive Gaussian noise (Kalman, 1960). As suggested above this “observer” function is probably located in the PPC (Andersen et al., 2010; Cui, 2016). A new class of emerging neural decoding algorithms are neural networks. Neural networks can model complex and nonlinear interactions, which is very desirable for decoding (Glaser et al., 2017). They are also particularly efficient in dealing with large datasets, which is advantageous given the ever-increasing number of neurons that we can simultaneously record. The drawback is a longer time (hours) required for training that is hardly compatible with a real application. Nevertheless, the potential is promising and several studies are ongoing (Burrow et al., 1997; Sussillo et al., 2016; Molano-Mazon et al., 2018; Rao, 2019).

Another crucial point is the detection of the intention to start the movement. In this study decoding of reach and grasp properties was pursued to reconstruct the movement but, a possible prosthesis would still miss the information about resting and action states. This information is necessary to trigger the movement of a prosthetic arm. Firing rates of neurons in PPC are modulated by the task states, neural activity is different for resting state, movement planning or actual movement (Cui and Andersen, 2007; Stetson and Andersen, 2015). This information can be used to instruct the decoder to detect transitions between planning to movement states (Shenoy et al., 2003). Also neurons in V6A exhibit this modulation (Santandrea et al., 2018), preliminary results show that movement intention can be decoded from V6A (Filippini et al., 2018), thus completing the set of information needed to potentially move a prosthetic arm.

Finally, functional MRI studies proposed a putative human homologue of area V6A (Pitzalis et al., 2013), which is likely located in the anterior part of the superior parieto-occipital cortex (aSPOC) (Gallivan and Culham, 2015). aSPOC shows enhanced visual activation to objects presented within the peripersonal space, even when the potential action is not actually executed (Gallivan et al., 2011a). Decoding of pre-movement activity of aSPOC with fMRI pattern analysis allowed reliable classification of specific actions that were subsequently performed, with a clear distinction between reaching and grasping movements (Gallivan et al., 2011b). This evidence points toward an area in the human brain which shares similar function with monkey area V6A.

## 6. Conclusions

Neurons in dorsomedial area V6A of macaque encode for several aspects of reach and grasp movements. In this thesis neural signals were decoded to reconstruct reaching goals and type of grips. Decoding is a critical step of Brain Computer Interfaces technology. BCIs aim to restore basic movements in patients who suffer of impaired movement due to spinal cord damage or other neurodegenerative disorders. Signals decoded from V6A are potentially adequate to control reaching and grasping components required to move a prosthetic arm. Furthermore, these results undermine the traditional view of two separate networks for reaching and grasping, both reach and grasp properties were decoded with high accuracy from V6A. This has intriguing application for BCIs: a single area is enough to extract information about the whole prehension act, with attractive advantages in term of implant invasiveness. The proposal of a human homologue of area V6A opens new perspectives for reach and grasp related signals that may be used to improve BCIs.

## 7. Bibliography

- Aflalo T, Kellis S, Klaes C, Lee B, Shi Y, Pejsa K, Shanfield K, Hayes-Jackson S, Aisen M, Heck C, Liu C, Andersen RA (2015) Neurophysiology. Decoding motor imagery from the posterior parietal cortex of a tetraplegic human. *Science* 348:906–910.
- Aggarwal V, Tenore F, Acharya S, Schieber MH, Thakor N V. (2009) Cortical decoding of individual finger and wrist kinematics for an upper-limb neuroprosthesis. In: Proceedings of the 31st Annual International Conference of the IEEE Engineering in Medicine and Biology Society: Engineering the Future of Biomedicine, EMBC 2009, pp 4535–4538.
- Allison T, McCarthy G, Wood CC, Jones SJ (1991) Potentials evoked in human and monkey cerebral cortex by stimulation of the median nerve: A review of scalp and intracranial recordings. *Brain* 114:2465–2503.
- Andersen RA, Burdick JW, Musallam S, Pesaran B, Cham JG (2004) Cognitive neural prosthetics. *Trends Cogn Sci* 8:486–493.
- Andersen RA, Hwang EJ, Mulliken GH (2010) Cognitive neural prosthetics. *Annu Rev Psychol* 61:169–190, C1-3.
- Andersen RA, Kellis S, Klaes C, Aflalo T (2014) Toward more versatile and intuitive cortical brain-machine interfaces. *Curr Biol* 24:R885-97.
- Anderson KD (2004) Targeting Recovery: Priorities of the Spinal Cord-Injured Population. *J Neurotrauma* 21:1371–1383.
- Baldauf D, Cui H, Andersen RA (2008) The Posterior Parietal Cortex Encodes in Parallel Both Goals for Double-Reach Sequences. *J Neurosci* 28:10081–10089.
- Bansal AK, Truccolo W, Vargas-Irwin CE, Donoghue JP (2012) Decoding 3D reach and grasp from hybrid signals in motor and premotor cortices: spikes, multiunit activity, and local field potentials. *J Neurophysiol* 107:1337–1355.
- Battaglia-Mayer A, Ferraina S, Genovesio A, Marconi B, Squatrito S, Molinari M, Lacquaniti F, Caminiti R (2001) Eye-hand coordination during reaching. II. An analysis of the relationships between visuomanual signals in parietal cortex and parieto-frontal association projections. *Cereb Cortex* 11:528–544.
- Battaglia-Mayer A, Ferraina S, Mitsuda T, Marconi B, Genovesio A, Onorati P, Lacquaniti F, Caminiti R (2000) Early Coding of Reaching in the Parietooccipital Cortex. *J Neurophysiol* 83:2374–2391.
- Battaglia-Mayer A, Mascaro M, Caminiti R (2007) Temporal evolution and strength of neural activity in parietal cortex during eye and hand movements. *Cereb Cortex* 17:1350–1363.
- Battaglini PP, Muzur A, Galletti C, Skrap M, Brovelli A, Fattori P (2002) Effects of lesions to area V6A in monkeys. *Exp Brain Res* 144:419–422.
- Beck JM, Ma WJ, Kiani R, Hanks T, Churchland AK, Roitman J, Shadlen MN, Latham PE, Pouget A (2008) Probabilistic Population Codes for Bayesian Decision Making. *Neuron* 60:1142–1152.
- Ben Hamed S, Schieber MH, Pouget A (2007) Decoding M1 neurons during multiple finger

movements. *J Neurophysiol* 98:327–333.

- Bockbrader MA, Francisco G, Lee R, Olson J, Solinsky R, Boninger ML (2018) Brain Computer Interfaces in Rehabilitation Medicine. *PM R* 10:S233–S243.
- Bokil HS, Pesaran B, Andersen RA, Mitra PP (2006) A Method for Detection and Classification of Events in Neural Activity. *IEEE Trans Biomed Eng* 53.
- Bosco A, Breveglieri R, Chinellato E, Galletti C, Fattori P (2010) Reaching activity in the medial posterior parietal cortex of monkeys is modulated by visual feedback. *J Neurosci* 30:14773–14785.
- Bosco A, Breveglieri R, Hadjidimitrakis K, Galletti C, Fattori P (2016) Reference frames for reaching when decoupling eye and target position in depth and direction. *Sci Rep* 6:21646.
- Bosco A, Breveglieri R, Reser D, Galletti C, Fattori P (2015) Multiple representation of reaching space in the medial posterior parietal area V6A. *Cereb Cortex* 25:1654–1667.
- Brandman DM, Cash SS, Hochberg LR (2017) Review: Human Intracortical Recording and Neural Decoding for Brain-Computer Interfaces. *IEEE Trans Neural Syst Rehabil Eng* 25:1687–1696.
- Breviglieri R, Bosco A, Galletti C, Passarelli L, Fattori P (2016) Neural activity in the medial parietal area V6A while grasping with or without visual feedback. *Sci Rep* 6:28893.
- Breviglieri R, De Vitis M, Bosco A, Galletti C, Fattori P (2018) Interplay Between Grip and Vision in the Monkey Medial Parietal Lobe. *Cereb Cortex* 28:2028–2042.
- Breviglieri R, Galletti C, Bosco A, Gamberini M, Fattori P (2015) Object affordance modulates visual responses in the macaque medial posterior parietal cortex. *J Cogn Neurosci* 27:1447–1455.
- Breviglieri R, Galletti C, Dal Bò G, Hadjidimitrakis K, Fattori P (2014) Multiple aspects of neural activity during reaching preparation in the medial posterior parietal area V6A. *J Cogn Neurosci* 26:878–895.
- Breviglieri R, Hadjidimitrakis K, Bosco A, Sabatini SP, Galletti C, Fattori P (2012) Eye position encoding in three-dimensional space: integration of version and vergence signals in the medial posterior parietal cortex. *J Neurosci* 32:159–169.
- Breviglieri R, Kutz DF, Fattori P, Gamberini M, Galletti C (2002) Somatosensory cells in the parieto-occipital area V6A of the macaque. *Neuroreport* 13:2113–2116.
- Burman KJ, Bakola S, Richardson KE, Reser DH, Rosa MGP (2014) Patterns of afferent input to the caudal and rostral areas of the dorsal premotor cortex (6DC and 6DR) in the marmoset monkey. *J Comp Neurol* 522:3683–3716.
- Burrow M, Dugger J, Humphrey DR, Reed DJ, Hochberg LR (1997) Cortical control of a robot using a time-delay neural network. *Int Conf Rehabil Robot*:83–86.
- Buzsáki G, Anastassiou CA, Koch C (2012) The origin of extracellular fields and currents--EEG, ECoG, LFP and spikes. *Nat Rev Neurosci* 13:407–420.
- Caminiti R, Ferraina S, Johnson PB (1996) The sources of visual information to the primate frontal lobe: A novel role for the superior parietal lobule. *Cereb Cortex* 6:319–328.
- Carmena JM, Lebedev MA, Crist RE, O'Doherty JE, Santucci DM, Dimitrov DF, Patil PG, Henriquez

- CS, Nicolelis MAL (2003) Learning to control a brain-machine interface for reaching and grasping by primates. *PLoS Biol* 1:E42.
- Carpaneto J, Raos V, Umiltà MA, Fogassi L, Murata A, Gallese V, Micera S (2012) Continuous decoding of grasping tasks for a prospective implantable cortical neuroprosthesis. *J Neuroeng Rehabil* 9:84.
- Carpaneto J, Umiltà M a., Fogassi L, Murata a., Gallese V, Micera S, Raos V (2011) Decoding the activity of grasping neurons recorded from the ventral premotor area F5 of the macaque monkey. *Neuroscience* 188:80–94.
- Chang SWC, Dickinson AR, Snyder LH (2008) Limb-Specific Representation for Reaching in the Posterior Parietal Cortex. *J Neurosci* 28:6128–6140.
- Chang SWC, Snyder LH (2012) The representations of reach endpoints in posterior parietal cortex depend on which hand does the reaching. *J Neurophysiol* 107:2352–2365.
- Chen J, Reitzen SD, Kohlenstein JB, Gardner EP (2009) Neural Representation of Hand Kinematics During Prehension in Posterior Parietal Cortex of the Macaque Monkey. *J Neurophysiol* 102:3310–3328.
- Chinellato E, del Pobil AP (2016) *The Visual Neuroscience of Robotic Grasping*. Cham: Springer International Publishing.
- Chinellato E, Grzyb BJ, Marzocchi N, Bosco A, Fattori P, del Pobil AP (2011) The Dorso-medial visual stream: From neural activation to sensorimotor interaction. *Neurocomputing* 74:1203–1212.
- Collinger JL, Wodlinger B, Downey JE, Wang W, Tyler-Kabara EC, Weber DJ, McMorland AJ, Velliste M, Boninger ML, Schwartz AB (2013) High-performance neuroprosthetic control by an individual with tetraplegia. *Lancet* 381:557–564.
- Cui H (2016) Forward Prediction in the Posterior Parietal Cortex and Dynamic Brain-Machine Interface. *Front Integr Neurosci* 10:35.
- Cui H, Andersen RA (2007) Posterior Parietal Cortex Encodes Autonomously Selected Motor Plans. *Neuron* 56:552–559.
- De Vitis M, Breveglieri R, Hadjidimitrakis K, Vanduffel W, Galletti C, Fattori P (2019) The neglected medial part of macaque area PE: segregated processing of reach depth and direction. *Brain Struct Funct* 224:2537–2557.
- Dea M, Hamadjida A, Elgbeili G, Quessy S, Dancause N (2016) Different Patterns of Cortical Inputs to Subregions of the Primary Motor Cortex Hand Representation in *Cebus apella*. *Cereb Cortex* 26:1747–1761.
- Donchin O, Gribova A, Steinberg O, Bergman H, Vaadia E (1998) Primary motor cortex is involved in bimanual coordination. *Nature* 395:274–278.
- Downey JE, Brane L, Gaunt RA, Tyler-Kabara EC, Boninger ML, Collinger JL (2017) Motor cortical activity changes during neuroprosthetic-controlled object interaction. *Sci Rep* 7:16947.
- Fani S, Bianchi M, Jain S, Pimenta Neto JS, Boege S, Grioli G, Bicchi A, Santello M (2016) Assessment of Myoelectric Controller Performance and Kinematic Behavior of a Novel Soft Synergy-Inspired Robotic Hand for Prosthetic Applications. *Front Neurobot* 10:11.

- Fattori P, Breveglieri R, Amoroso K, Galletti C (2004) Evidence for both reaching and grasping activity in the medial parieto-occipital cortex of the macaque. *Eur J Neurosci* 20:2457–2466.
- Fattori P, Breveglieri R, Bosco A, Gamberini M, Galletti C (2017) Vision for prehension in the medial parietal cortex. *Cereb Cortex* 27:1149–1163.
- Fattori P, Breveglieri R, Marzocchi N, Filippini D, Bosco A, Galletti C (2009) Hand orientation during reach-to-grasp movements modulates neuronal activity in the medial posterior parietal area V6A. *J Neurosci* 29:1928–1936.
- Fattori P, Breveglieri R, Raos V, Bosco A, Galletti C (2012) Vision for action in the macaque medial posterior parietal cortex. *J Neurosci* 32:3221–3234.
- Fattori P, Gamberini M, Kutz DF, Galletti C (2001) “Arm-reaching” neurons in the parietal area V6A of the macaque monkey. *Eur J Neurosci* 13:2309–2313.
- Fattori P, Kutz DF, Breveglieri R, Marzocchi N, Galletti C (2005) Spatial tuning of reaching activity in the medial parieto-occipital cortex (area V6A) of macaque monkey. *Eur J Neurosci* 22:956–972.
- Fattori P, Raos V, Breveglieri R, Bosco A, Marzocchi N, Galletti C (2010) The dorsomedial pathway is not just for reaching: grasping neurons in the medial parieto-occipital cortex of the macaque monkey. *J Neurosci* 30:342–349.
- Ferraina S, Garasto MR, Battaglia-Mayer A, Ferraresi P, Johnson PB, Lacquaniti F, Caminiti R (1997) Visual control of hand-reaching movement: activity in parietal area 7m. *Eur J Neurosci* 9:1090–1095.
- Fetz EE (2007) Volitional control of neural activity: implications for brain-computer interfaces. *J Physiol* 579:571–579.
- Filippini M, Breveglieri R, Akhras MA, Bosco A, Chinellato E, Fattori P (2017) Decoding Information for Grasping from the Macaque Dorsomedial Visual Stream. *J Neurosci* 37:4311–4322.
- Filippini M, Morris A, Hadjimitsakis K, Breveglieri R, Fattori P (2018) Population decoding reveals a rapid transition from visuospatial to hand motor processing in macaque medial parietal area V6A. Available at: <https://www.abstractsonline.com/pp8/#!/4649/presentation/34806>.
- Flanders M, Cordo PJ (1989) Kinesthetic and visual control of a bimanual task: specification of direction and amplitude. *J Neurosci* 9:447–453.
- Flint RD, Lindberg EW, Jordan LR, Miller LE, Slutzky MW (2012) Accurate decoding of reaching movements from field potentials in the absence of spikes. *J Neural Eng* 9:046006.
- Gail A, Andersen R (2006) Neural Dynamics in Monkey Parietal Reach Region Reflect Context-Specific Sensorimotor Transformations. *J Neurosci* 26:9376–9384.
- Gallese V, Murata A, Kaseda M, Niki N, Sakata H (1994) Deficit of hand preshaping after muscimol injection in monkey parietal cortex. *Neuroreport* 5:1525–1529.
- Galletti C, Battaglini PP, Fattori P (1995) Eye Position Influence on the Parieto-occipital Area PO (V6) of the Macaque Monkey. *Eur J Neurosci* 7:2486–2501.
- Galletti C, Fattori P (2018) The dorsal visual stream revisited: Stable circuits or dynamic pathways? *Cortex* 98:203–217.

- Galletti C, Fattori P, Gamberini M, Kutz DF (1999a) The cortical visual area V6: brain location and visual topography. *Eur J Neurosci* 11:3922–3936.
- Galletti C, Fattori P, Kutz DF, Gamberini M (1999b) Brain location and visual topography of cortical area V6A in the macaque monkey. *Eur J Neurosci* 11:575–582.
- Galletti C, Kutz DF, Gamberini M, Breveglieri R, Fattori P (2003) Role of the medial parieto-occipital cortex in the control of reaching and grasping movements. In: *Experimental brain research*, pp 158–170.
- Gallivan JP, Culham JC (2015) Neural coding within human brain areas involved in actions. *Curr Opin Neurobiol* 33:141–149.
- Gallivan JP, Goodale MA (2018) The dorsal “action” pathway. In: *Handbook of clinical neurology*, pp 449–466.
- Gallivan JP, McLean A, Culham JC (2011a) Neuroimaging reveals enhanced activation in a reach-selective brain area for objects located within participants’ typical hand workspaces. *Neuropsychologia* 49:3710–3721.
- Gallivan JP, McLean DA, Valyear KF, Pettypiece CE, Culham JC (2011b) Decoding action intentions from preparatory brain activity in human parieto-frontal networks. *J Neurosci* 31:9599–9610.
- Gamberini M, Galletti C, Bosco A, Breveglieri R, Fattori P (2011) Is the Medial Posterior Parietal Area V6A a Single Functional Area? *J Neurosci* 31:5145–5157.
- Gao Y, Black M J, Bienenstock E, Shoham S, Donoghue JP (2002) Probabilistic Inference of Hand Motion from Neural Activity in Motor Cortex. In: *Advances in Neural Information Processing Systems 14*. The MIT Press.
- Gardner EP (2017) Neural pathways for cognitive command and control of hand movements. *Proc Natl Acad Sci U S A* 114:4048–4050.
- Gardner EP, Babu KS, Reitzen SD, Ghosh S, Brown AS, Chen J, Hall AL, Herzlinger MD, Kohlenstein JB, Ro JY (2007) Neurophysiology of Prehension. I. Posterior Parietal Cortex and Object-Oriented Hand Behaviors. *J Neurophysiol* 97:387–406.
- Gautrais J, Thorpe S (1998) Rate coding versus temporal order coding: A theoretical approach. In: *BioSystems*, pp 57–65.
- Georgopoulos A, Kalaska J, Caminiti R, Massey J (1982) On the relations between the direction of two-dimensional arm movements and cell discharge in primate motor cortex. *J Neurosci* 2:1527–1537.
- Gilja V, Pandarinath C, Blabe CH, Nuyujukian P, Simeral JD, Sarma AA, Sorice BL, Perge JA, Jarosiewicz B, Hochberg LR, Shenoy K V, Henderson JM (2015) Clinical translation of a high-performance neural prosthesis. *Nat Med* 21:1142–1145.
- Glaser JJ, Chowdhury RH, Perich MG, Miller LE, Kording KP (2017) Machine learning for neural decoding.
- Goodale MA, Milner AD (1992) Separate visual pathways for perception and action. *Trends Neurosci* 15:20–25.
- Graf ABA, Andersen RA (2014) Brain–machine interface for eye movements. *Proc Natl Acad Sci*

111:17630–17635.

- Hadjidimitrakis K, Bakola S, Wong YT, Hagan MA (2019) Mixed Spatial and Movement Representations in the Primate Posterior Parietal Cortex. *Front Neural Circuits* 13:15.
- Hadjidimitrakis K, Bertozzi F, Breveglieri R, Bosco A, Galletti C, Fattori P (2014a) Common neural substrate for processing depth and direction signals for reaching in the monkey medial posterior parietal cortex. *Cereb Cortex* 24:1645–1657.
- Hadjidimitrakis K, Bertozzi F, Breveglieri R, Fattori P, Galletti C (2014b) Body-Centered, Mixed, but not Hand-Centered Coding of Visual Targets in the Medial Posterior Parietal Cortex During Reaches in 3D Space. *Cereb Cortex* 24:3209–3220.
- Hadjidimitrakis K, Bertozzi F, Breveglieri R, Galletti C, Fattori P (2017) Temporal stability of reference frames in monkey area V6A during a reaching task in 3D space. *Brain Struct Funct* 222:1959–1970.
- Hadjidimitrakis K, Breveglieri R, Bosco A, Fattori P (2012) Three-dimensional eye position signals shape both peripersonal space and arm movement activity in the medial posterior parietal cortex. *Front Integr Neurosci* 6:37.
- Hadjidimitrakis K, Breveglieri R, Placenti G, Bosco A, Sabatini SP, Fattori P (2011) Fix your eyes in the space you could reach: neurons in the macaque medial parietal cortex prefer gaze positions in peripersonal space. *Gribble PL, ed. PLoS One* 6:e23335.
- Hadjidimitrakis K, Dal Bo' G, Breveglieri R, Galletti C, Fattori P (2015) Overlapping representations for reach depth and direction in caudal superior parietal lobule of macaques. *J Neurophysiol* 114:2340–2352.
- Hatsopoulos N, Joshi J, O'Leary JG (2004) Decoding continuous and discrete motor behaviors using motor and premotor cortical ensembles. *J Neurophysiol* 92:1165–1174.
- Hatsopoulos NG, Donoghue JP (2009) The science of neural interface systems. *Annu Rev Neurosci* 32:249–266.
- Hauschild M, Mulliken GH, Fineman I, Loeb GE, Andersen RA (2012) Cognitive signals for brain-machine interfaces in posterior parietal cortex include continuous 3D trajectory commands. *Proc Natl Acad Sci U S A* 109:17075–17080.
- Hayhoe MM, Shrivastava A, Mruczek R, Pelz JB (2003) Visual memory and motor planning in a natural task. *J Vis* 3:6.
- Hochberg LR, Bacher D, Jarosiewicz B, Masse NY, Simeral JD, Vogel J, Haddadin S, Liu J, Cash SS, van der Smagt P, Donoghue JP (2012) Reach and grasp by people with tetraplegia using a neurally controlled robotic arm. *Nature* 485:372–375.
- Hochberg LR, Serruya MD, Friehs GM, Mukand JA, Saleh M, Caplan AH, Branner A, Chen D, Penn RD, Donoghue JP (2006) Neuronal ensemble control of prosthetic devices by a human with tetraplegia. *Nature* 442:164–171.
- Hotson G, Smith RJ, Rouse AG, Schieber MH, Thakor N V., Wester BA (2016) High Precision Neural Decoding of Complex Movement Trajectories Using Recursive Bayesian Estimation with Dynamic Movement Primitives. *IEEE Robot Autom Lett* 1:676–683.
- Hwang EJ, Andersen R a (2013) The utility of multichannel local field potentials for brain-machine

interfaces. *J Neural Eng* 10:046005.

Jarosiewicz B, Chase SM, Fraser GW, Velliste M, Kass RE, Schwartz AB (2008) Functional network reorganization during learning in a brain-computer interface paradigm. *Proc Natl Acad Sci U S A* 105:19486–19491.

Jeannerod M (1986) Mechanisms of visuomotor coordination: A study in normal and brain-damaged subjects. *Neuropsychologia* 24:41–78.

Jeannerod M (1997) The cognitive neuroscience of action. *Trends Cogn Sci* 1:238.

Jeannerod M, Decety J (1995) Mental motor imagery: a window into the representational stages of action. *Curr Opin Neurobiol* 5:727–732.

Kalman RE (1960) A New Approach to Linear Filtering and Prediction Problems. *J Basic Eng* 82:35.

Kandel E, Schwartz J, Jessel T, Siegelbaum S, Hudspeth AJ (2013) *Principles of Neural Science*, Fifth Edition.

Katyal KD, Johannes MS, Kellis S, Aflalo T, Klaes C, McGee TG, Para MP, Shi Y, Lee B, Pejsa K, Liu C, Wester BA, Tenore F, Beaty JD, Ravitz AD, Andersen RA, McLoughlin MP (2014) A collaborative BCI approach to autonomous control of a prosthetic limb system. In: *Conference Proceedings - IEEE International Conference on Systems, Man and Cybernetics*, pp 1479–1482.

Kemere C, Santhanam G, Yu BM, Afshar A, Ryu SI, Meng TH, Shenoy K V. (2008) Detecting Neural-State Transitions Using Hidden Markov Models for Motor Cortical Prostheses. *J Neurophysiol* 100:2441–2452.

Kim HK, Biggs SJ, Schloerb DW, Carmena JM, Lebedev MA, Nicolelis MAL, Srinivasan MA (2006) Continuous shared control for stabilizing reaching and grasping with brain-machine interfaces. *IEEE Trans Biomed Eng* 53:1164–1173.

Kim S-P, Simeral JD, Hochberg LR, Donoghue JP, Black MJ (2008) Neural control of computer cursor velocity by decoding motor cortical spiking activity in humans with tetraplegia. *J Neural Eng* 5:455–476.

Klaes C, Kellis S, Aflalo T, Lee B, Pejsa K, Shanfield K, Hayes-Jackson S, Aisen M, Heck C, Liu C, Andersen RA (2015) Hand Shape Representations in the Human Posterior Parietal Cortex. *J Neurosci* 35:15466–15476.

Kozai TDY, Jaquins-Gerstl AS, Vazquez AL, Michael AC, Cui XT (2015) Brain Tissue Responses to Neural Implants Impact Signal Sensitivity and Intervention Strategies. *ACS Chem Neurosci* 6:48–67.

Kravitz DJ, Peng CS, Baker CI (2011) Real-World Scene Representations in High-Level Visual Cortex: It's the Spaces More Than the Places. *J Neurosci* 31:7322–7333.

Kutz DF, Marzocchi N, Fattori P, Cavalcanti S, Galletti C (2005) Real-Time Supervisor System Based on Trinary Logic to Control Experiments With Behaving Animals and Humans. *J Neurophysiol* 93:3674–3686.

Lehmann SJ, Scherberger H (2013) Reach and gaze representations in macaque parietal and premotor grasp areas. *J Neurosci* 33:7038–7049.

- Luppino G, Ben Hamed S, Gamberini M, Matelli M, Galletti C (2005) Occipital (V6) and parietal (V6A) areas in the anterior wall of the parieto-occipital sulcus of the macaque: A cytoarchitectonic study. *Eur J Neurosci* 21:3056–3076.
- Ma WJ, Beck JM, Latham PE, Pouget A (2006) Bayesian inference with probabilistic population codes. *Nat Neurosci* 9:1432–1438.
- Marzocchi N, Breveglieri R, Galletti C, Fattori P (2008) Reaching activity in parietal area V6A of macaque: eye influence on arm activity or retinocentric coding of reaching movements? *Eur J Neurosci* 27:775–789.
- Matelli M, Luppino G (2001) Parietofrontal Circuits for Action and Space Perception in the Macaque Monkey. *Neuroimage* 14:S27–S32.
- Mattar E (2013) A survey of bio-inspired robotics hands implementation: New directions in dexterous manipulation. *Rob Auton Syst* 61:517–544.
- McGuire LMM, Sabes PN (2011) Heterogeneous Representations in the Superior Parietal Lobule Are Common across Reaches to Visual and Proprioceptive Targets. *J Neurosci* 31:6661–6673.
- Milekovic T, Truccolo W, Grün S, Riehle A, Brochier T (2015) Local field potentials in primate motor cortex encode grasp kinetic parameters. *Neuroimage* 114:338–355.
- Milner D, Goodale M (2006) *The Visual Brain in Action*. Oxford University Press.
- Molano-Mazon M, Onken A, Piasini E, Panzeri S (2018) Synthesizing realistic neural population activity patterns using Generative Adversarial Networks. :1–24.
- Mulliken GH, Musallam S, Andersen RA (2008a) Decoding trajectories from posterior parietal cortex ensembles. *J Neurosci* 28:12913–12926.
- Mulliken GH, Musallam S, Andersen RA (2008b) Forward estimation of movement state in posterior parietal cortex. *Proc Natl Acad Sci* 105:8170–8177.
- Murata A, Gallese V, Luppino G, Kaseda M, Sakata H (2000) Selectivity for the Shape, Size, and Orientation of Objects for Grasping in Neurons of Monkey Parietal Area AIP. *J Neurophysiol* 83:2580–2601.
- Murphy MD, Guggenmos DJ, Bundy DT, Nudo RJ (2016) Current Challenges Facing the Translation of Brain Computer Interfaces from Preclinical Trials to Use in Human Patients. *Front Cell Neurosci* 9.
- Musallam S, Corneil BD, Greger B, Scherberger H, Andersen R (2004) Cognitive control signals for neural prosthetics. *Science* 305:258–262.
- National Spinal Cord Injury Statistical Center, Birmingham A (2018) Annual Statistical Report. Available at: <https://www.nscisc.uab.edu/>.
- Neggers SF, Bekkering H (2001) Gaze anchoring to a pointing target is present during the entire pointing movement and is driven by a non-visual signal. *J Neurophysiol* 86:961–970.
- Nelissen K, Fiave PA, Vanduffel W (2018) Decoding Grasping Movements from the Parieto-Frontal Reaching Circuit in the Nonhuman Primate. *Cereb Cortex* 28:1245–1259.
- Nicolelis MAL, Lebedev MA (2009) Principles of neural ensemble physiology underlying the operation of brain-machine interfaces. *Nat Rev Neurosci* 10:530–540.

- Paninski L, Fellows MR, Hatsopoulos NG, Donoghue JP (2004) Spatiotemporal Tuning of Motor Cortical Neurons for Hand Position and Velocity. *J Neurophysiol* 91:515–532.
- Pitzalis S, Sereno MI, Committeri G, Fattori P, Galati G, Tosoni A, Galletti C (2013) The human homologue of macaque area V6A. *Neuroimage* 82:517–530.
- Quian Quiroga R, Snyder LH, Batista AP, Cui H, Andersen RA (2006) Movement Intention Is Better Predicted than Attention in the Posterior Parietal Cortex. *J Neurosci* 26:3615–3620.
- Raiguel SE, Xiao D-K, Marcar VL, Orban GA (1999) Response Latency of Macaque Area MT/V5 Neurons and Its Relationship to Stimulus Parameters. *J Neurophysiol* 82:1944–1956.
- Rao RP (2019) Towards neural co-processors for the brain: combining decoding and encoding in brain–computer interfaces. *Curr Opin Neurobiol* 55:142–151.
- Raos V, Umiltá M-A, Gallese V, Fogassi L (2004) Functional properties of grasping-related neurons in the dorsal premotor area F2 of the macaque monkey. *J Neurophysiol* 92:1990–2002.
- Rizzolatti G, Matelli M (2003) Two different streams form the dorsal visual system: Anatomy and functions. In: *Experimental Brain Research*, pp 146–157.
- Rupp R (2014) Challenges in clinical applications of brain computer interfaces in individuals with spinal cord injury. *Front Neuroeng* 7.
- Rus D, Tolley MT (2015) Design, fabrication and control of soft robots. *Nature* 521:467–475.
- Sakata H, Taira M, Kusunoki M, Murata A, Tanaka Y (1997) The TINS Lecture The parietal association cortex in depth perception and visual control of hand action. *Trends Neurosci* 20:350–357.
- Sakata H, Taira M, Mine S, Murata A (2012) Hand-Movement-Related Neurons of the Posterior Parietal Cortex of the Monkey: Their Role in the Visual Guidance of Hand Movements. In: *Control of Arm Movement in Space*, pp 185–198. Springer-Verlag.
- Sakata H, Taira M, Murata A, Mine S (1995) Neural Mechanisms of Visual Guidance of Hand Action in the Parietal Cortex of the Monkey. *Cereb Cortex* 5:429–438.
- Salatino JW, Ludwig KA, Kozai TDY, Purcell EK (2017) Glial responses to implanted electrodes in the brain. *Nat Biomed Eng* 1:862–877.
- Sandberg K, Andersen LM, Overgaard M (2014) Using multivariate decoding to go beyond contrastive analyses in consciousness research. *Front Psychol* 5:1250.
- Santandrea E, Breveglieri R, Bosco A, Galletti C, Fattori P (2018) Preparatory activity for purposeful arm movements in the dorsomedial parietal area V6A: Beyond the online guidance of movement. *Sci Rep* 8:6926.
- Santello M, Bianchi M, Gabbicini M, Ricciardi E, Salvietti G, Prattichizzo D, Ernst M, Moscatelli A, Jorntell H, Kappers AML, Kyriakopoulos K, Schaeffer AA, Castellini C, Bicchi A (2016) Towards a synergy framework across neuroscience and robotics: Lessons learned and open questions. Reply to comments on: “Hand synergies: Integration of robotics and neuroscience for understanding the control of biological and artificial hands.” *Phys Life Rev* 17:54–60.
- Santhanam G, Ryu SI, Yu BM, Afshar A, Shenoy K V (2006) A high-performance brain-computer interface. *Nature* 442:195–198.

- Schaffelhofer S, Agudelo-Toro A, Scherberger H (2015) Decoding a wide range of hand configurations from macaque motor, premotor, and parietal cortices. *J Neurosci* 35:1068–1081.
- Schaffelhofer S, Scherberger H (2016) Object vision to hand action in macaque parietal, premotor, and motor cortices. *Elife* 5.
- Scherberger H (2009) Neural control of motor prostheses. *Curr Opin Neurobiol* 19:629–633.
- Scherberger H, Jarvis MR, Andersen RA (2005) Cortical local field potential encodes movement intentions in the posterior parietal cortex. *Neuron* 46:347–354.
- Schmolesky MT, Wang Y, Hanes DP, Thompson KG, Leutgeb S, Schall JD, Leventhal a G (1998) Signal timing across the macaque visual system. *J Neurophysiol* 79:3272–3278.
- Schwartz A (1994) Direct cortical representation of drawing. *Science* (80- ) 265:540–542.
- Schwartz AB (2016) *Movement: How the Brain Communicates with the World*. *Cell* 164:1122–1135.
- Schwartz AB, Cui XT, Weber D, Moran DW (2006) Brain-Controlled Interfaces: Movement Restoration with Neural Prosthetics. *Neuron* 52:205–220.
- Serruya M, Hatsopoulos N, Fellows M, Paninski L, Donoghue J (2003) Robustness of neuroprosthetic decoding algorithms. *Biol Cybern* 88:219–228.
- Serruya MD, Hatsopoulos NG, Paninski L, Fellows MR, Donoghue JP (2002) Instant neural control of a movement signal. *Nature* 416:141–142.
- Shenoy K V., Kaufman MT, Sahani M, Churchland MM (2011) A dynamical systems view of motor preparation. Implications for neural prosthetic system design. *Prog Brain Res* 192:33–58.
- Shenoy K V., Kureshi SA, Pesaran B, Buneo CA, Andersen RA, Meeker D, Batista AP, Cao S, Burdick JW, Mitra PP (2003) Neural prosthetic control signals from plan activity. *Neuroreport* 14:591–596.
- Simeral JD, Kim S-P, Black MJ, Donoghue JP, Hochberg LR (2011) Neural control of cursor trajectory and click by a human with tetraplegia 1000 days after implant of an intracortical microelectrode array. *J Neural Eng* 8:025027.
- Simpson LA, Eng JJ, Hsieh JTC, Wolfe and the Spinal Cord Injury Re DL (2012) The Health and Life Priorities of Individuals with Spinal Cord Injury: A Systematic Review. *J Neurotrauma* 29:1548–1555.
- Snyder LH, Batista a P, Andersen R a (1997) Coding of intention in the posterior parietal cortex. *Nature* 386:167–170.
- Sofroniew M V. (2018) Dissecting spinal cord regeneration. *Nature* 557:343–350.
- Spinks RL, Kraskov A, Brochier T, Umilta MA, Lemon RN (2008) Selectivity for Grasp in Local Field Potential and Single Neuron Activity Recorded Simultaneously from M1 and F5 in the Awake Macaque Monkey. *J Neurosci* 28:10961–10971.
- Stark E, Asher I, Abeles M (2007) Encoding of reach and grasp by single neurons in premotor cortex is independent of recording site. *J Neurophysiol* 97:3351–3364.

- Stavisky SD, Kao JC, Nuyujukian P, Ryu SI, Shenoy K V (2015) A high performing brain–machine interface driven by low-frequency local field potentials alone and together with spikes. *J Neural Eng* 12:036009.
- Stein RB, Gossen ER, Jones KE (2005) Neuronal variability: noise or part of the signal? *Nat Rev Neurosci* 6:389–397.
- Stetson C, Andersen RA (2015) Early planning activity in frontal and parietal cortex in a simplified task. *J Neurophysiol*.
- Sussillo D, Kao JC, Ryu SI, Shenoy K V., Stavisky SD (2016) Making brain-machine interfaces robust to future neural variability. *Nat Commun* 7:1–12.
- Taira M, Mine S, Georgopoulos AP, Murata A, Sakata H (1990) Parietal cortex neurons of the monkey related to the visual guidance of hand movement. *Exp Brain Res* 83:29–36.
- Taylor DM, Tillery SIH, Schwartz AB (2002) Direct cortical control of 3D neuroprosthetic devices. *Science* 296:1829–1832.
- Thorpe S, Fize D, Marlot C (1996) Speed of processing in the human visual system. *Nature* 381:520–522.
- Thorpe SJ (1990) Spike arrival times: A highly efficient coding scheme for neural networks. *Biol Comput A Phys Choice*:91–94.
- Torres EB, Quiñero R, Cui H, Buneo CA (2013) Neural correlates of learning and trajectory planning in the posterior parietal cortex. *Front Integr Neurosci* 7:39.
- Townsend BR, Subasi E, Scherberger H (2011) Grasp Movement Decoding from Premotor and Parietal Cortex. *J Neurosci* 31:14386–14398.
- Ungerleider LG, Mishkin M (1982) Two cortical visual systems. *Anal Vis Behav*:549–586.
- Vargas-Irwin CE, Shakhnarovich G, Yadollahpour P, Mislow JMK, Black MJ, Donoghue JP (2010) Decoding complete reach and grasp actions from local primary motor cortex populations. *J Neurosci* 30:9659–9669.
- Velliste M, Perel S, Spalding M, Whitford A, Schwartz A (2008) Cortical control of a robotic arm for self-feeding. *Nature* 453:1098–1101.
- Waldert S (2016) Invasive vs. Non-Invasive Neuronal Signals for Brain-Machine Interfaces: Will One Prevail? *Front Neurosci* 10.
- Wessberg J, Stambaugh CR, Kralik JD, Beck PD, Laubach M, Chapin JK, Kim J, Biggs SJ, Srinivasan M a, Nicolelis M a (2000) Real-time prediction of hand trajectory by ensembles of cortical neurons in primates. *Nature* 408:361–365.
- Whitlock JR (2017) Posterior parietal cortex. *Curr Biol* 27:R691–R695.
- Wise SP, Boussaoud D, Johnson PB, Caminiti R (1997) Premotor and parietal cortex: corticocortical connectivity and combinatorial computations. *Annu Rev Neurosci* 20:25–42.
- Wodlinger B, Downey JE, Tyler-Kabara EC, Schwartz AB, Boninger ML, Collinger JL (2015) Ten-dimensional anthropomorphic arm control in a human brain–machine interface: difficulties, solutions, and limitations. *J Neural Eng* 12:016011.

Wolpert DM, Miall RC (1996) Forward Models for Physiological Motor Control. *Neural Netw* 9:1265–1279.

Young W (2014) Spinal Cord Regeneration. *Cell Transplant* 23:573–611.

Zhang H (2004) The Optimality of Naive Bayes. *Proc Seventeenth Int Florida Artif Intell Res Soc Conf FLAIRS 2004* 1:1–6.

Zhuang J, Truccolo W, Vargas-Irwin C, Donoghue JP (2010) Reconstructing grasping motions from high-frequency local field potentials in primary motor cortex. *Conf Proc . Annu Int Conf IEEE Eng Med Biol Soc IEEE Eng Med Biol Soc Annu Conf* 2010:4347–4350.